NEURAL REGENERATION RESEARCH
www.nrronline.org

Research Article

Siponimod exerts neuroprotective effects on the retina and higher visual pathway through neuronal S1PR1 in experimental glaucoma

Devaraj Basavarajappa*, Vivek Gupta*, Nitin Chitranshi, Roshana Vander Wall, Rashi Rajput, Kanishka Pushpitha, Samridhi Sharma, Mehdi Mirzaei, Alexander Klistorner, Stuart L. Graham

https://doi.org/10.4103/1673-5374.344952

Date of submission: January 7, 2022

Date of decision: March 1, 2022

Date of acceptance: June 6, 2022

Date of web publication: September 16, 2022

From the Contents

Graphical Abstract

Neuroprotective effects of siponimod mediated through neuronal S1PR1 in ON injury condition

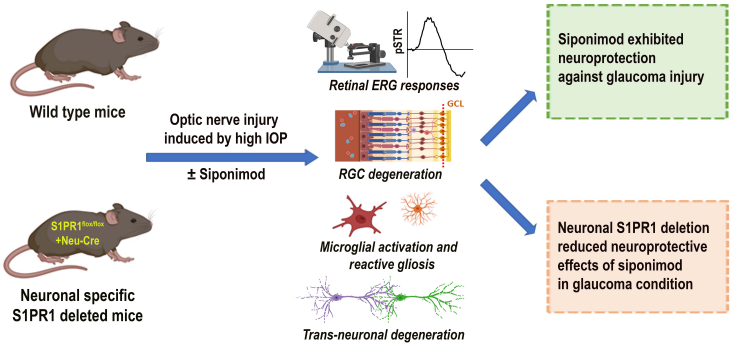

Abstract

Sphingosine-1-phosphate receptor (S1PR) signaling regulates diverse pathophysiological processes in the central nervous system. The role of S1PR signaling in neurodegenerative conditions is still largely unidentified. Siponimod is a specific modulator of S1P1 and S1P5 receptors, an immunosuppressant drug for managing secondary progressive multiple sclerosis. We investigated its neuroprotective properties *in vivo* on the retina and the brain in an optic nerve injury model induced by a chronic increase in intraocular pressure or acute N-methyl-D-aspartate excitotoxicity. Neuronal-specific deletion of sphingosine-1-phosphate receptor (S1PR1) was carried out by expressing AAV-PHP.eB-Cre recombinase under Syn1 promoter in S1PR1$^{flox/flox}$ mice to define the role of S1PR1 in neurons. Inner retinal electrophysiological responses, along with histological and immunofluorescence analysis of the retina and optic nerve tissues, indicated significant neuroprotective effects of siponimod when administered orally via diet in chronic and acute optic nerve injury models. Further, siponimod treatment showed significant protection against trans-neuronal degenerative changes in the higher visual center of the brain induced by optic nerve injury. Siponimod treatment also reduced microglial activation and reactive gliosis along the visual pathway. Our results showed that siponimod markedly upregulated neuroprotective Akt and Erk1/2 activation in the retina and the brain. Neuronal-specific deletion of S1PR1 enhanced retinal and dorsolateral geniculate nucleus degenerative changes in a chronic optic nerve injury condition and attenuated protective effects of siponimod. In summary, our data demonstrated that S1PR1 signaling plays a vital role in the retinal ganglion cell and dorsolateral geniculate nucleus neuronal survival in experimental glaucoma, and siponimod exerts direct neuroprotective effects through S1PR1 in neurons in the central nervous system independent of its peripheral immuno-modulatory effects. Our findings suggest that neuronal S1PR1 is a neuroprotective therapeutic target and its modulation by siponimod has positive implications in glaucoma conditions.

Key Words: glaucoma; intraocular pressure; neurodegeneration; neuroprotection; optic nerve injury; retinal ganglion cells; siponimod; sphingosine-1-phosphate

Introduction

Sphingosine-1-phosphate (S1P) is a crucial lipid signaling molecule generated from ceramide metabolism and binds to five G-protein-coupled receptors, termed S1P1–5 receptors (S1PR1–5) (O'Sullivan and Dev, 2017). S1PRs are expressed ubiquitously and play major roles in cell survival, growth, migration, and differentiation. Consequently, S1PR modulation has emerged as a potential therapeutic strategy in various diseases, including inflammatory, cardiovascular, and brain disorders (Cartier and Hla, 2019). Siponimod (BAF312) and fingolimod (FTY720) are S1P structural analogues that modulate S1P receptor signaling and are approved immunosuppressive drugs for the treatment of multiple sclerosis (MS) (Kappos et al., 2006, 2018; Gajofatto, 2017). The active form, fingolimod-phosphate (fingolimod-P), formed following *in vivo* phosphorylation, binds potently to four S1P receptors, S1P1, S1P3, S1P4, and S1P5. Siponimod, in contrast, is a selective modulator of S1P1 and S1P5 receptors. Immunomodulation has been primarily regarded as the mechanism of action of both drugs in MS. Modulation of S1PR in lymphocytes by these drugs prevents their egress from secondary lymphoid organs and consequently infiltration into the CNS, reducing inflammation (Kappos et al., 2006; Chun et al., 2019).

The CNS cells express four out of the five S1PRs (S1P1, S1P2, S1P3, and S1P5) (Healy and Antel, 2016), though the expression levels vary depending on the cell type and the injury stimulus (Healy and Antel, 2016; Karunakaran and van Echten-Deckert, 2017; Lucaciu et al., 2020). A growing body of evidence shows that S1PR signaling is implicated in the pathophysiology of various disorders of the CNS. S1PRs in neuronal precursor cells and neurons play roles in cell migration, neurogenesis, neural development, and survival (Gupta et al., 2012; Karunakaran and van Echten-Deckert, 2017). S1PR signaling pathways in microglia and astrocytes regulate their activation, proliferation, gliosis, and neuroinflammation (Lucaciu et al., 2020). S1PRs in oligodendroglia and oligodendrocyte precursor cells participate in differentiation, survival, and myelination (Martin and Sospedra, 2014; Roggeri et al., 2020). Siponimod, in addition to immunomodulatory effects on the peripheral immune cells, can cross the blood-brain barrier (Hunter et al., 2016; Kipp, 2020; Bigaud et al., 2021). Recent data on the protective effects of siponimod in clinical trials

Department of Clinical Medicine, Faculty of Medicine, Health and Human Sciences, Macquarie University, North Ryde, Sydney, NSW, Australia
***Correspondence to:** Devaraj Basavarajappa, PhD, devaraj.basavarajappa@mq.edu.au; Vivek Gupta, PhD, vivek.gupta@mq.edu.au.
https://orcid.org/0000-0003-0997-0196 (Devaraj Basavarajappa); https://orcid.org/0000-0002-0202-7843 (Vivek Gupta)

Funding: *This investigator-initiated study grant (to SLG) was funded by Novartis, Australia. The investigators also like to acknowledge the funding support from the National Health and Medical Research Council (NHMRC) of Australia, Perpetual Hilcrest, Ophthalmic Research Institute of Australia (ORIA) and Macquarie University, NSW, Australia.*
How to cite this article: *Basavarajappa D, Gupta V, Chitranshi N, Wall RV, Rajput R, Pushpitha K, Sharma S, Mirzaei M, Klistorner A, Graham SL (2023) Siponimod exerts neuroprotective effects on the retina and higher visual pathway through neuronal S1PR1 in experimental glaucoma. Neural Regen Res 18(4):840-848.*

involving secondary progressive MS patients suggests that siponimod may directly interact with S1PRs in the CNS (Behrangi et al., 2019; Dumitrescu et al., 2019) which is important as secondary progressive MS is largely driven by local CNS degenerative mechanisms (Baecher-Allan et al., 2018; Simkins et al., 2021). There is limited evidence to demonstrate the *in vivo* role of S1PRs in the CNS cell types in degenerative conditions.

The retina and optic nerve (ON) are considered unique extensions of the CNS and show specific changes in response to various neurological disorders (London et al., 2013). Glaucoma is an age-related multifactorial neurodegenerative disease, clinically characterized by cupping of the optic nerve head with irreversible visual field loss due to ON damage and retinal ganglion cell (RGC) death, with anterograde trans-neuronal degeneration in higher visual centers (Jonas et al., 2017; Mélik Parsadaniantz et al., 2020). The major risk factor for the development and progression of glaucoma is elevated intraocular pressure (IOP) (Pang and Clark, 2020). Elevated IOP causes axonal transport disruption, microvascular abnormalities, extracellular matrix remodeling, glial activation, and ultimately RGCs degeneration (You et al., 2013; Artero-Castro et al., 2020; Rolle et al., 2020). Based on the above discussion, we hypothesized that targeting neuronal S1PR1 by siponimod could produce neuroprotective effects in glaucoma conditions, independent of the drug's peripheral immunosuppressive effects. The present study investigated the neuroprotective effect of siponimod on the visual pathway in glaucomatous conditions using combined physiological, structural, and biochemical measures. Further, we established the role of S1PR1 in RGCs survival, ON damage, and trans-neuronal degeneration in higher visual centers and the drug-mediated effects using cell-specific S1PR1 ablated mice.

Methods

Experimental animals

All animal experiments in this study were conducted in compliance with the Australian Code of Practice for the Care and Use of Animals for Scientific Purposes and the guidelines of the ARVO (the Association for Research in Vision and Ophthalmology) Statement for the Use of Animals in Ophthalmic and Vision Research and approved by Macquarie University Animal Ethics Committee (AEC Reference No. 2018/018) approved on June 28, 2018. Wild-type C57BL/6 mice (4–6 weeks, body weight 16–20 g) were purchased from Animal Resources Centre, Perth, Australia. B6.129S6(FVB)-S1pr1$^{tm2.1Rlp}$/J mice (4–6 weeks, body weight 16–20 g, RRID: IMSR_JAX:019141) were obtained from the Jackson Laboratory (Bar Harbor, ME, USA). Mice were bred under specific pathogen-free conditions at the Animal Care Facility of Macquarie University. All animals were maintained in an air-conditioned room with a controlled temperature (21–28°C) and fixed daily 12-hour light/dark cycles. The animals were randomly divided into four groups (10 mice in each group): (1) control (sham, normal IOP) group, (2) control (sham, normal IOP) group with siponimod treatment, (3) high IOP/NMDA (N-methyl-D-aspartate) excitotoxicity subjected untreated group and (4) high IOP/NMDA excitotoxicity subjected group with siponimod treatment. Before assigning, we first examined 4–6 week-old mouse eyes for abnormality, including topical fluorescein assessment using ophthalmoscope/magnifying loupes. The initial baseline electrophysiological responses, electroretinogram (ERG), and positive scotopic threshold response (pSTR) were also measured to ensure the normal health status of the animal eyes. Siponimod (BAF312) was obtained from Novartis (Basel, Switzerland) and administered to recipient mice through a dose of 10 mg/kg incorporated in the diet and fed *ad libitum*, and 3–4 mice per cage were maintained. This dose was chosen based on previously optimized dose-dependent effects of siponimod in rodent models (Dietrich et al., 2018). Diet loaded with 10 mg/kg siponimod was suggested as an optimized dose for long-term preclinical studies to get maximum drug effects (approximately equivalent to a daily drug intake of 30 µg/mouse when considering a mean daily food uptake of ~3 g/d) (Bigaud et al., 2021).

Induction of elevated IOP by intracameral microbead injections

Elevation of IOP was induced by injection of polystyrene microspheres (10-µm diameter FluoSpheres; Invitrogen, Carlsbad, CA, USA) into the anterior chamber of the eyes as described previously (You et al., 2014; Chitranshi et al., 2019; Abbasi et al., 2020, 2021). Briefly, mice were anesthetized with intraperitoneal injections of ketamine (75 mg/kg) (Provet Pty Ltd, Erskine Park, NSW, Australia) and medetomidine (0.5 mg/kg) (Troy Laboratories Pty Ltd, Glendenning, NSW, Australia) and the body temperature was maintained using a warming pad throughout the experimental procedure. After pupils were dilated with topical 1% tropicamide, topical anesthetic drops (Alcaine-proxymetacaine 0.5%, Alcon Laboratories Pty Ltd, Macquarie Park, NSW, Australia) were applied prior to injections. Intracameral injections were performed with 2 µL of polystyrene microspheres (3.6×10^6 microbeads/mL) using a Hamilton syringe connected to a disposable 33G needle (TSK Laboratory, Tochigi, Japan). All procedures were performed using an operating microscope (OPMI Vario S88, Carl Zeiss, Oberkochen, Germany), and care was taken to avoid needle contact with the iris or lens. One of the eyes was randomly selected for ocular injection, leaving the other eye as contralateral intra-animal control. An equivalent volume of sterile phosphate-buffered saline (PBS) was injected into the eyes of control (sham) mice, and these animals served as the control group (normal IOP). Anesthesia was reversed by subcutaneous atipamezole (0.75 mg/kg) injection and 0.3% ciprofloxacin drops (Ciloxan; Alcon Laboratories Pty Ltd) and 0.1% dexamethasone eye drops (Maxidex, Novartis Pharmaceuticals Australia Pty Ltd, Macquarie Park, NSW, Australia) were applied to the injected eyes. Lacrilube (Allergan Australia Pty Ltd, Gordon, NSW, Australia) was then applied to the cornea. Microbead injection was performed weekly between weeks 0 and 4 and then fortnightly until week 8. The IOP was monitored regularly using an iCare TonoLab rebound tonometer (Icare Tonovet, Helsinki, Finland) as described previously (Chitranshi et al., 2019; Abbasi et al., 2020; Mirzaei et al., 2020).

Electroretinographic analysis

Scotopic electroretinographic recordings were performed as described previously using the Ganzfeld ERG system (Phoenix Research Laboratories, Pleasanton, CA, USA) (Joly et al., 2017; Rodriguez et al., 2018). Mice were dark-adapted overnight and anesthetized with ketamine and medetomidine (75 and 0.5 mg/kg, respectively) and placed on a warming pad. Pupils were dilated using 1% tropicamide, and topical anesthetic (Alcaine, Alcon Laboratories Pty Ltd) drops were applied to the cornea under dim red light. The ground and reference electrodes were inserted into the tail and subcutaneously into the forehead of the animal, respectively. The body temperature of the animals was maintained at around 37°C with an electric heating pad during recordings. The recording electrode (gold-plate objective lens) was placed on the eye's corneal surface after applying hypromellose to maintain proper contact between the cornea and the electrode to record ERGs. After stabilizing the baseline in darkness, the ERG responses were recorded from each eye individually. ERGs were recorded using a flash intensity of 6.1 log cd·s/m^2. Dim stimulation (–4.3 log cd·s/m^2) was delivered 30 times at a frequency of 0.5 Hz. The amplitude of positive scotopic threshold response (pSTR) was measured from baseline to the positive peak observed around 120 ms.

Intravitreal NMDA injection

Retinal neurotoxicity was induced by a single intravitreal injection of NMDA (30 nmol per eye) (Dheer et al., 2019). Mice were anesthetized in an induction chamber with 2–5% isoflurane in oxygen, and then animals were maintained on 1–3% isoflurane in oxygen (0.6–1 L/min flow of oxygen) on a warming pad during the procedure. After pupils were dilated with 1% tropicamide, a single amount of 3 µL NMDA (Sigma-Aldrich, St. Louis, MO, USA) solution in sterile PBS was administered using a 33G needle into the vitreous chamber behind the lens. The control animal group eyes were injected with an equivalent volume of sterile PBS. All injections were performed under an operating surgical microscope (OPMI Vario S88, Carl Zeiss). At 7 days after NMDA injection, inner retinal electrophysiological recordings were performed by measuring pSTR responses, and animals were sacrificed by cervical dislocation to harvest the tissues for analysis.

Viral injections

Adeno-associated viruses (AAVs), stereotype AAV-PHP.eB (Vector Biolabs, USA) harboring Cre recombinase under neuron-specific promoter hSyn1 (AAV-PHP.eB-Syn1-GFP-Cre and AAV-PHP.eB-Syn1-GFP as control) or oligodendrocyte specific promoter, MBP (myelin basic protein) (AAV-PHP.eB-MBP-GFP-Cre and AAV-PHP.eB-MBP-GFP as control) were systemically delivered through tail vein injection into S1PR1$^{flox/flox}$ transgenic mice 1 week before inducing elevated IOPs. Adult mice of 4–5 weeks old were anesthetized and maintained in 1–3% isoflurane in oxygen on a warming pad as stated above during viral injections. Mice were injected with 50 µL AAV viral suspension (1.5×10^{11} vg) manually into a lateral tail vein using a 33G needle attached to the Hamilton syringe. Tails were warmed before injection in 40°C water for 1 minute and cleaned with 70% alcohol pads, prior to viral vector delivery.

Immunofluorescence staining

Mice were euthanized by cervical dislocation, and the brain, eyes, and ON tissues were harvested from the animals after transcardial perfusion with PBS and 4% paraformaldehyde. Postfixed tissues were then embedded in optimal cutting temperature compound (OCT) (Sakura Finetek, Torrance, CA, USA) in dry ice. ON were dissected approximately 1 mm anterior to the optic nerve head and embedded vertically in OCT. Seven-micrometer thick sagittal retinal cryosections were cut for eyes, 3-µm thick cross-sections were cut for optic nerves, and 15-µm thick serial coronal sections were cut for brains using Leica CM1950 cryo section equipment (Leica Biosystems, Nussloch, Germany). The coronal plane sections between –2.05 to –2.20 mm from Bregma were used for staining (Bertacchi et al., 2019; You et al., 2019). Cryosections or deparaffined sections (after antigen retrieval) were treated with a blocking buffer containing 0.3% Triton X-100 and 5% serum of the secondary species (donkey) (Sigma-Aldrich) in PBS for 2 hours at room temperature. The tissue sections were then incubated with primary antibodies overnight at 4°C. The following primary antibodies were used for immunofluorescence staining: rabbit anti-Iba1 (Ionized calcium-binding adaptor molecule 1) (microglial marker; 1:1500; 019-19741, FUJIFILM Wako Shibayagi, Cat# 019-19741, RRID: AB_839504); rabbit anti-GFAP (glial fibrillary acidic protein) (a marker for reactive gliosis; 1:1500; Agilent, Santa Clara, CA, USA, Cat# Z0334, RRID:AB_10013382), rabbit anti-GFP (green fluoresce protein) (a reporter marker; 1:500; Abcam, Vic, Australia, Cat# ab290, RRID: AB_303395) and mouse anti-NeuN (neuronal marker; 1:1000; Abcam, Cat# ab104224, RRID: AB_10711040) and mouse anti-phosphorylated neurofilament heavy-chain (pNFH) (optic nerve damage marker; 1:1000; BioLegend-SMI-31, San Diego, CA, USA, BioLegend, Cat# 801601, RRID: AB_2564641). After primary antibody incubation, the sections were washed with PBS four times and incubated with appropriate secondary antibodies with a dilution of 1:500 at room temperature for 1 hour (Cy3-AffiniPure donkey anti-rabbit IgG (H+L), Jackson ImmunoResearch Labs, West Grove, PA, USA, Cat# 711-165-152, RRID: AB_2307443 or Alexa Fluor 488-AffiniPure donkey anti-mouse IgG

(H+L), Jackson ImmunoResearch Labs, Cat# 715-545-150, RRID: AB_2340846), washed and mounted with anti-fade mounting media with Prolong 4′,6-diamidino-2-phenylindole (DAPI; Life Technologies, Eugene, OR, USA). All images were acquired using a Zeiss fluorescence microscope (ZEISS Axio Imager Z2, Carl Zeiss). The pNFH$^+$ area and glial activation were measured from the immunofluorescence images of three-four cross-sections of each animal's optic nerve using ImageJ software (version 1.52; NIH, Bethesda, MD, USA; Schneider et al., 2012). Three to four sections of medial dorsolateral geniculate nucleus (dLGN) from each animal brain were chosen for imaging and quantification of NeuN-positive cells in dLGN using ImageJ software.

Histology

Post-fixed eye and brain tissues were processed via an automatic tissue processor (Leica ASP200S, Leica Biosystems) and embedded in paraffin wax. Tissue marking dye was used to ensure identical eye orientation. Paraffin sections (7-µm thick) of retinal specimens comprised the whole retina cut through the optic nerve head (parasagittal plane containing the superior and the inferior retina within the width of the ON) and were stained with hematoxylin and eosin (H and E). Images were captured using Zeiss Microscope (ZEISS Axio Imager Z2) and analyzed with ImageJ. The number of cells in the ganglion cell layer (GCL) was counted over a length of 500 µm (100 to 600 µm from the edge of the optic disc). Cell counts were obtained from three consecutive sections of each animal eye and averaged to analyze the number of cells in the GCL. For brain tissue, serial coronal paraffin sections (10 µm thick) comprising medial dLGN sections (between –2.05 to –2.20 mm from Bregma) from each animal brain were chosen for Nissl blue staining. Briefly, the deparaffined brain sections were hydrated with ethanol gradient and stained with cresyl violet (0.5%) for 5 minutes, and rinsed with water before mounting. Stained sections were imaged using Zeiss Microscope (ZEISS Axio Imager Z2, Carl Zeiss) and the viable Nissl positive neurons with visible nuclei were counted using ImageJ. Neuron densities were measured from three to four consecutive sections of each animal in the dLGN region of the brain.

Western blot analysis

Harvested tissue samples were snap-frozen in liquid nitrogen and subsequently resuspended in ice-cold lysis buffer (20 mM Tris-HCl, pH 8.0, 1% Triton X-100, 2 mM EDTA, 2 mM PMSF, 100 mM NaCl, 1 mM Na_3VO_4, 0.1% SDS and complete protease inhibitor cocktail). Tissue samples (retina and microdissected dLGN of the brain) were then homogenized by sonication and centrifuged at 10,000 × *g* for 10 minutes at 4°C to collect the protein supernatant. The protein concentration of the lysates was quantified by Micro BCA assay (Thermo Fisher Scientific, Waltham, MA, USA). Proteins (around 20 µg) were resolved by SDS-PAGE and transferred to nitrocellulose membrane by electroblotting (Invitrogen iBlot2, Thermo Fisher Scientific). Membranes were blocked with non-fat dry milk powder (5%) in TTBS (20 mM Tris-HCl pH 7.4, 100 mM NaCl, and 0.1% Tween 20) for 1 hour at room temperature and incubated with primary antibodies overnight at 4°C. The primary antibodies used were: rabbit monoclonal anti-phospho-Akt (Ser473) (1:1000; (D9E) XP 4060, Cell Signaling Technology, Danvers, MA, USA, Cat# 4060, RRID: AB_2315049), rabbit monoclonal anti-Akt (1:1000; 11E7 (pan), Cell Signaling Technology, Cat# 4685, RRID: AB_2225340), rabbit monoclonal anti-phospho-p44/42 MAPK (Erk1/2) (Thr202/Tyr204) (1:1000; (20G11), Cell Signaling Technology, Cat# 4376, RRID: AB_331772), and rabbit monoclonal anti-p44/42 MAPK (Erk1/2) (1:1000; (137F5), Cell Signaling Technology, Cat# 4695, RRID: AB_390779); rabbit polyclonal anti-GFP (1:1000; Abcam, Cat# ab290, RRID: AB_303395), rabbit polyclonal anti-S1P1/EDG1 (1:1000; Abcam, Cat# ab11424, RRID: AB_298029) and mouse monoclonal anti-β-actin (1:5000; Abcam, Cat# ab6276, RRID: AB_2223210); rabbit polyclonal anti-Iba1 (1:1000; FUJIFILM Wako Shibayagi, Cat# 019-19741, RRID: AB_839504); rabbit polyclonal anti-GFAP (1:1500; Agilent, Z0334, RRID: AB_10013382). The membranes were then washed and incubated for 1 hour at room temperature with a secondary antibody conjugated to horseradish peroxidase (goat anti-rabbit 1:5000, Thermo Fisher Scientific, Cat# 31460, RRID: AB_228341 and goat anti-mouse 1:5000, Thermo Fisher Scientific, Cat# 62-6520, RRID: AB_2533947). After washing, the protein bands were detected by enhanced chemiluminescence (Super Signal West Femto Maximum Sensitive Substrate; Thermo Fisher Scientific) according to the manufacturer's instructions, and images were captured with a Bio-Rad ChemiDoc^{MP} Imaging system (Bio-Rad Laboratories, Inc., Hercules, CA, USA). The mean densitometry analysis of band intensities was determined after relative expression of the proteins normalized to β-actin using ImageJ software.

Statistical analysis

Statistical analysis of the data in this study was performed as described previously (Chitranshi et al., 2019; Abbasi et al., 2020) using GraphPad Prism 8 software (GraphPad Software Inc., San Diego, CA, USA, www.graphpad.com). The animals subjected to four experimental groups were utilized to analyze the retinal electrophysiological (pSTR amplitudes) changes, optic nerve damage, histology, western blotting, and immunofluorescence staining of the tissues. The number of samples (*n*) indicated in each figure represents the tissues from the different animals of the same group. Comparisons between the groups were performed by one-way analysis of variance followed by Tukey's multiple comparisons test. All the data are presented as mean ± standard deviation of the mean (SD) for given *n* sizes. A *P*-value < 0.05 was considered statistically significant for data analysis.

Results

Siponimod preserves retinal structure and function in optic nerve injury models

The potential protective effects of siponimod on inner retinal function and structure were measured in a high IOP mouse model (**Figure 1A**). For functional assessment of the inner retina, we measured the pSTR amplitudes (You et al., 2013). Siponimod-treated mice with intracameral injections of microbeads showed elevated IOPs comparable to the untreated control animals (**Figure 1B**). After 8 weeks, the high IOP subjected eyes exhibited a decline in pSTR amplitudes, while mice treated with siponimod (10 mg/kg in the diet and fed *ad libitum*) showed significant protection against the pSTR amplitude loss ($P < 0.01$; **Figure 1C** and **D**).

Assessment of cellular changes in the ganglion cell layer (GCL) and ON damage was then performed. Histological analysis of the retinal sections stained with H and E revealed a significant decrease in the number of cells in GCL in high IOP subjected untreated mice eyes compared with the control normal IOP (sham) mice eyes ($P < 0.001$). GCL loss was significantly attenuated in the siponimod-treated mice group compared with the untreated mice group in high IOP conditions, where GCL cell density loss decreased from 60.64 ± 8.73% to 25.29 ± 8.21% ($P < 0.001$; **Figure 1E** and **F**). Neurofilament heavy chain in RGC axons has been reported to undergo dephosphorylation in eyes subjected to elevated IOP (Kashiwagi et al., 2003; Chidlow et al., 2011). Immunofluorescence staining of ON cross-sections with phosphorylated neurofilament heavy chain (pNFH) antibody and pNFH$^+$ area measurements revealed a significant decrease in pNFH immunoreactivity in high IOP ONs. This ON axonal damage in elevated IOP conditions was decreased from 64.88 ± 8.25% to 38.21 ± 9.15% with siponimod treatment compared with the untreated mice ($P < 0.01$; **Figure 1G** and **H**). These results indicated that siponimod exerts neuroprotective effects on the retina and ON against neurodegenerative changes induced by chronic high IOP.

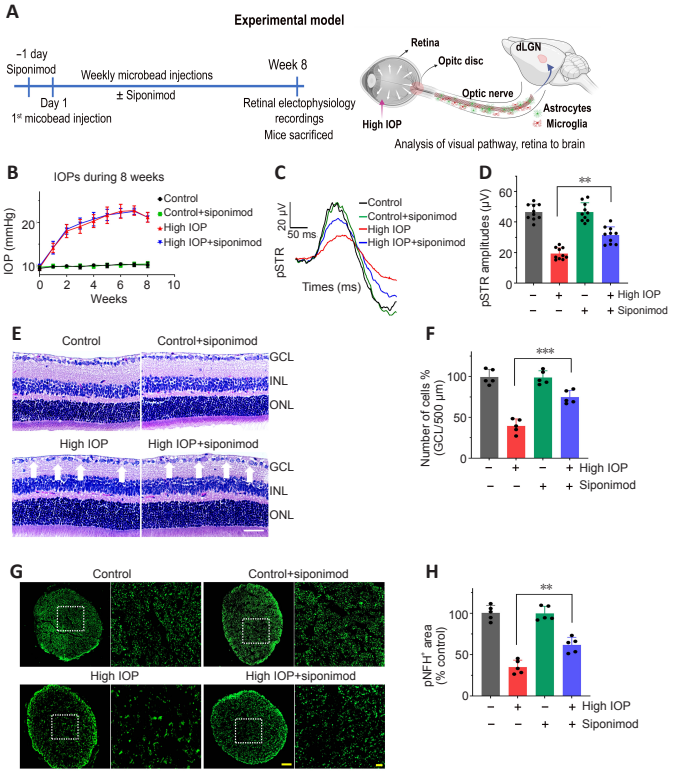

Figure 1 | Neuroprotective effects of siponimod on function and structure of the retina and optic nerve (ON) in high intraocular pressure (IOP) condition.
(A) Schematic depicting the experimental design and analysis of visual pathway in ON injury model. dLGN: Dorsolateral geniculate nucleus. (B) Chronic elevation of IOP in C57BL/6 mice eyes was induced by intracameral microbead injections for 2 months. (C) Positive scotopic threshold responses (pSTR) of control and glaucomatous mice eyes treated with/without siponimod after 8 weeks of chronic elevated IOP. (D) Quantification of the pSTR amplitudes (**$P < 0.01$, $n = 10$ per group). (E) Hematoxylin and eosin staining of sagittal cross-section of the eyes (representative images, arrows indicate the changes in cell densities, scale bar: 50 µm. GCL: Ganglion cell layer; INL: inner nuclear layer; ONL: outer nuclear layer). (F) Cell density in the GCL from the retinal hematoxylin and eosin-stained images (***$P < 0.001$, $n = 5$ per group). (G) Immunofluorescence staining of ON cross-sections (scale bar: 50 µm) with pNFH (SIM-31) and immunoreactivity measurements (green, pNFH$^+$ areas) from high magnified areas (boxes, scale bar: 10 µm) of ONs, and (H) their quantifications (**$P < 0.01$, $n = 5$ per group). Statistical significance was determined using one-way analysis of variance with Tukey's multiple comparisons test (mean ± SD).

The neuroprotective effect of siponimod on the retina was further tested in an acute NMDA excitotoxicity model. A significant retinal functional deterioration in response to NMDA toxicity was observed after 7 days post-injury. The pSTR amplitudes in NMDA-treated mice were reduced by 65.33 ± 3.78%, and this reduction was significantly protected with siponimod treatment ($P < 0.05$; **Figure 2A** and **B**). H and E staining of retinal sections and examination of ONs stained with pNFH further revealed the protective effects of siponimod. NMDA-induced cell loss in GCL decreased from 71.36 ± 9.61% to 47.58 ± 11.50% in the siponimod treated group compared with the untreated mice group ($P < 0.05$; **Figure 2C** and **D**). Axonal damage assessed by pNFH$^+$ area measurements showed pNFH immunoreactivity loss was decreased from 51.39 ± 10.99% to 22.02 ± 10.74% in siponimod treated mice in NMDA excitotoxicity condition compared with the untreated mice group ($P < 0.05$; **Figure 2E** and **F**). These results emphasize the protective effects of siponimod treatment on the retina in the NMDA injury model.

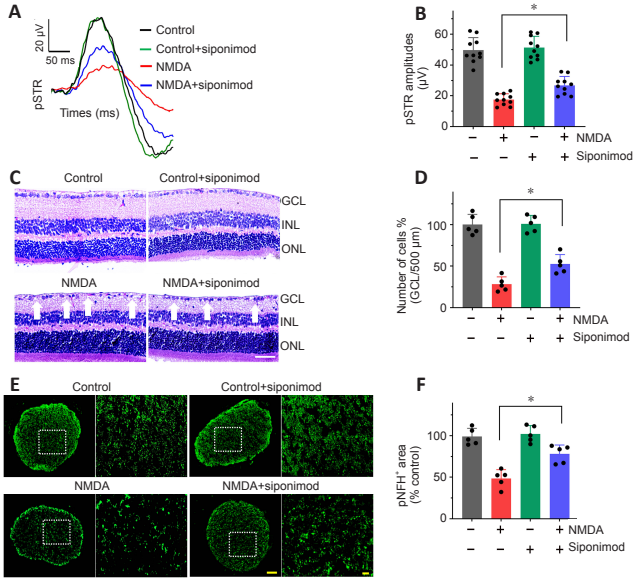

Figure 2 | Neuroprotective effects of siponimod on function and structure of the retina and optic nerve (ON) against acute retinal N-methyl-D-aspartate (NMDA) excitotoxicity.

(A) Positive scotopic threshold responses (pSTR) of the eyes after 7 days of NMDA excitotoxicity and (B) quantification of the pSTR amplitudes in acute retinal NMDA excitotoxicity (*$P < 0.05$, $n = 10$ per group). (C) Histological analysis of sagittal cross-sectional of the eyes stained with hematoxylin and eosin (representative images, arrows indicate the changes in cell densities, scale bar: 50 μm; GCL: ganglion cell layer; INL: inner nuclear layer; ONL: outer nuclear layer) and (D) cell counts in the GCL (*$P < 0.05$, $n = 5$ per group). (E) Immunofluorescence images of ON cross-sections stained with pNFH (green, representative, scale bar: 50 μm) and immunoreactivity measurements from magnified areas (boxes, scale bars: 10 μm) and (F) their quantitative analysis (*$P < 0.05$, $n = 5$ per group). Statistical significance was determined using one-way analysis of variance with Tukey's multiple comparisons test (mean ± SD).

Protective effects of siponimod on trans-neuronal degenerative changes in dLGN

Neuronal degenerative changes in the dLGN have been documented in ON injury conditions (Gupta et al., 2007; Yücel and Gupta, 2008; Sriram et al., 2012). The effect of siponimod on trans-neuronal degeneration under chronic elevated IOP in the dLGN region of the brain was evaluated by staining coronal brain sections with Nissl blue and NeuN. Quantitative neuronal cell density analysis revealed a significant protective effect of siponimod on neuronal cell loss in the dLGN. A decline of 38.95 ± 7.26% in neuronal cell density was observed in high IOP mice, and this degeneration was reduced to 12.53 ± 7.85% ($P < 0.01$) in the siponimod treated group compared with the untreated mice group (**Figure 3A** and **B**). Further, in high IOP eyes, the frequency of NeuN$^+$ cells was decreased by 39.34 ± 6.77%, whereas this loss was reduced to only 13.72 ± 7.36% in the siponimod treated group (**Figure 3C** and **D**). The higher visual cortex (V1) analysis in this high IOP condition for 2 months period showed no significant trans-neuronal degenerative changes. These results together establish a significant protective effect of siponimod on the neuronal cell population in the dLGN region of the brain.

Siponimod upregulates pro-survival signaling pathways

Phosphatidylinositol-3 kinase (PI3K)/Akt and the mitogen-activated protein kinase (Erk1/2) signaling play a critical role in neuron survival (Rai et al., 2019; Xu et al., 2020). FTY720 treatment has been shown to promote Akt/Erk activation in cultured neuronal cells and *in vivo* conditions (Zhang and Wang, 2020). Akt and Erk1/2 phosphorylation levels were evaluated by western blotting. A decrease in Akt and Erk phosphorylation levels was observed under high IOP conditions in the retina and dLGN region of the brain. Mice treated with siponimod showed significantly enhanced Akt ($P < 0.01$) and Erk1/2 phosphorylation in the retina ($P < 0.01$) and the dLGN ($P < 0.01$ for Erk1; $P < 0.001$ for Erk2; **Figure 4A** and **B**) compared with the untreated mice group in high IOP conditions.

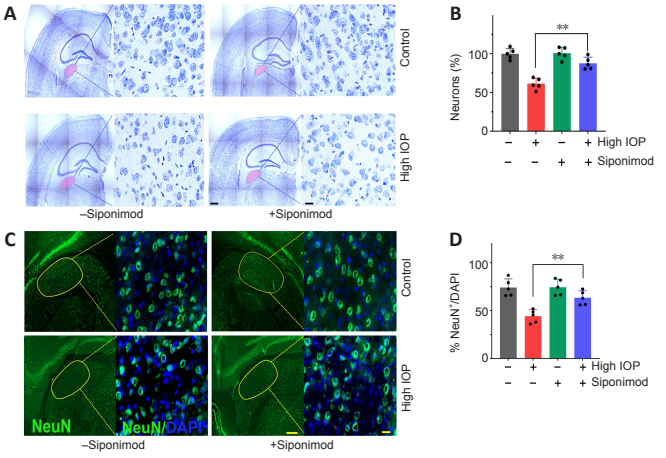

Figure 3 | Protective effects of siponimod on the dorsolateral geniculate nucleus (dLGN) of the brain in chronic glaucoma condition (8 weeks).

(A) Nissl staining of coronal sections (contralateral) of mouse brains (dLGN is marked, representative images, scale bar: 500 μm). (B) Neuronal density measured from magnified images (scale bar: 20 μm) of the dLGN. (C) Immunofluorescence images of coronal sections of mouse brains (contralateral, representative) stained with anti-NeuN (green) a neuronal marker and DAPI (blue) (scale bar: 200 μm), the dLGN region is marked. (D) Percentage of NeuN$^+$ cells out of DAPI-positive cells in the dLGN from magnified areas (scale bar: 20 μm). **$P < 0.01$, one-way analysis of variance with Tukey's multiple comparisons test, $n = 5$ per group.

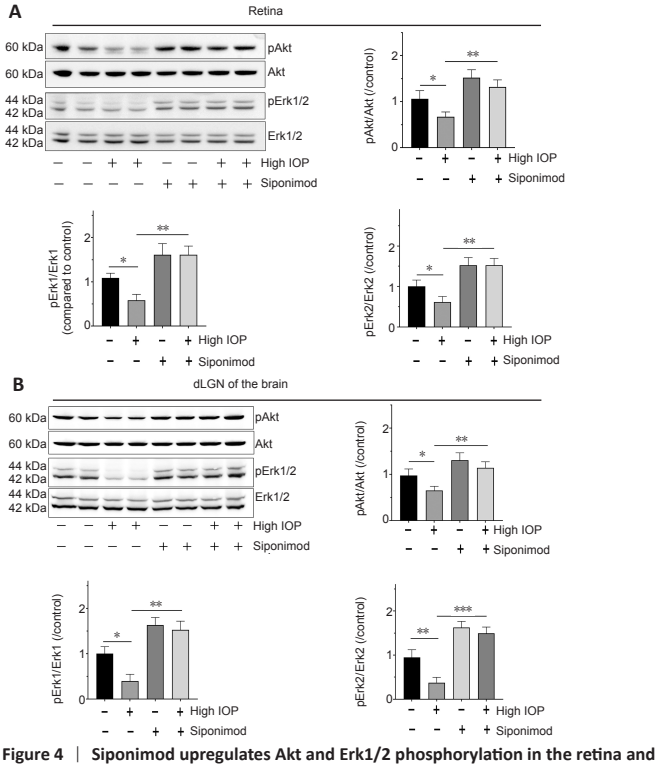

Figure 4 | Siponimod upregulates Akt and Erk1/2 phosphorylation in the retina and the brain.

(A) Western blot analysis of Akt (phsopho-S473 antibody) and Erk1/2 (phospho-p44/42 MAPK (Erk1/2) (Thr202/Tyr204) phosphorylation levels in retinas and (B) in the dorsolateral geniculate nucleus (dLGN) of the brain tissues lysates (8 weeks of chronic elevated IOP) and their densitometric quantitative analysis (*$P < 0.05$, **$P < 0.01$, ***$P < 0.001$, one-way analysis of variance with Tukey's multiple comparisons test, $n = 4$ per group).

Siponimod reduces microglial activation and reactive gliosis in the glaucoma model

Chronic neuroinflammation in glaucoma is implicated as an important component in disease pathogenesis. The early reactivity of glial cells (microglial activation and reactive gliosis) has been observed in the retina (Mélik Parsadaniantz et al., 2020; Rolle et al., 2020). Glial activation along the visual pathway was evaluated by investigating Iba1 and GFAP expression alterations. Immunofluorescence staining of the retina, ON, and the brain tissue sections with Iba1 and GFAP revealed activation of glial cells along the visual pathway in chronic high IOP condition (**Figure 5** and **Additional Figure 1**). Activated microglia in the retina, ON, and dLGN were reduced with siponimod treatment in chronic high IOP conditions (**Figure 5A**, **C** and

Additional Figure 1A). Microglial activation in the ON evaluated by measuring changes in Iba1$^+$ areas indicated a significant increase (3.02 ± 0.29-fold) of Iba1 immunoreactivity in the high IOP model. This activation was reduced in the siponimod-treated group to 1.84 ± 0.41 fold (**Additional Figure 1A**). Western blot analysis of retinal and dLGN tissues for Iba1 expression revealed a 3.63 ± 0.25-fold increase in the retina and 2.43 ± 0.32-fold increase in dLGN in high IOP conditions, and this upregulation was significantly diminished with siponimod treatment (2.27 ± 0.31-fold in retina and 1.63 ± 0.22-fold in dLGN) (**Figure 5B** and **D**).

In control retinas, GFAP immunoreactivity was primarily confined to the GCL. High IOP retinas showed GFAP labeling as a dense network of Müller cell processes in the GCL along with the emergence of a radial pattern of GFAP immunopositivity (**Figure 5E**). Similar hypertrophic reactive astrogliosis with upregulated GFAP was observed in ON (**Additional Figure 1B**) and dLGN of high IOP subjected mice (**Figure 5G**). This reactive gliosis was diminished with siponimod treatment. Western blot quantitative analysis of GFAP expression in the retina and dLGN tissues showed 4.33 ± 0.35-fold and 2.96 ± 0.27-fold upregulation, respectively in high IOP conditions compared with the control normal IOP (sham) mice group. Siponimod treatment resulted in its suppression to 2.23 ± 0.31-fold in the retina and 1.65 ± 0.23-fold in dLGN compared with the untreated mice (**Figure 5F** and **H**). GFAP immunoreactivity in the ON was increased to 3.47 ± 0.5-fold in high IOP condition compared with the control normal IOP (sham) mice but was reduced significantly to 1.96 ± 0.30 fold in siponimod treated mice ($P < 0.001$; **Additional Figure 1B**). These results indicated that the siponimod treatment effectively reduced microglial activation and reactive gliosis in chronic high IOP experimental glaucoma.

S1PR1 loss in RGCs and neurons exacerbates glaucoma injury attenuating siponimod protective effects

To define the role of S1PR1 intrinsic signaling in neuronal survival and its involvement in mediating the protective effects of the drug in glaucoma conditions, neuronal-specific ablation of S1PR1 was carried out in S1PR1$^{flox/flox}$ mice. The Cre-recombinase under neuron-specific promoter, Syn1 was integrated into AAV-PHP.eB vector and viral vectors were administered intravenously to S1PR1$^{flox/flox}$ mice (**Additional Figure 2A**). Efficient delivery of AAV construct crossing the blood-brain barrier was evident by GFP expression in the neuronal cells of mice receiving AAV injections. The transduction efficiency measured by the ratio of GFP$^+$ cells to the total NeuN$^+$ cells achieved 83.20 ± 7.63% for GFP control and 82.36 ± 6.87 for Cre recombinase AAVs in the dLGN regions of the brain. Similarly, the transduction efficiency of 76.93 ± 4.73% for GFP control and 75.31 ± 5.53% for Cre AAVs was observed for RGCs in the retina (**Additional Figure 2B–D**). Western blot analysis of dLGN and retinal tissues further validated the loss of S1PR1 expression in AAV-Cre recombinase-expressing mice. Densitometric quantification demonstrated that the S1PR1 expression in AAV-GFP-Cre injected mice was decreased by 67.95 ± 7.15% in the dLGN and about 61.43 ± 7.79% in the retina compared with the AAV-GFP injected control mice ($P <$ 0.0001; **Additional Figure 2E** and **F**).

The mice injected with AAV-GFP referred to as S1PR1$^{+/+}$ control mice (AAV-GFP) and the neuron-specific S1PR1 deleted mice (termed as Neu-S1PR$^{-/-}$ mice (AAV-GFP-Cre)) were administered siponimod diet (**Additional Figure 3**). No significant functional or structural changes were observed in the retina upon neuronal S1PR1 ablation under normal conditions. However, upon microbead-induced ON injury, neuronal S1PR1 ablated mice showed a significant decrease in the pSTR amplitudes and GCL thinning. Interestingly, the protective effects of siponimod were significantly attenuated in the group subjected to neuronal S1PR1 impairment (Neu-S1PR$^{-/-}$, AAV-GFP-Cre) compared with control S1PR$^{+/+}$ animals (AAV-GFP). High IOP-induced pSTR amplitude loss of 57.69 ± 5.03% was reduced to 32.58 ± 4.57% in siponimod-treated S1PR$^{+/+}$ control animals. However, NeuN-S1PR1$^{-/-}$ animals exhibited 77.62 ± 2.74% loss in high IOP eyes compared with 66.43 ± 2.45% loss in the siponimod treated group ($P < 0.01$; **Figure 6A–C**).

Further, quantitative analysis of the GCL from H and E stained retinal sections revealed a significant decrease ($P < 0.05$) in GCL density in Neu-S1PR1$^{-/-}$ ablated (AAV-GFP-Cre) mice compared with S1PR1$^{+/+}$ control (AAV-GFP) mice in high IOP conditions. The siponimod-mediated protective effect was significantly diminished in Neu-S1PR1$^{-/-}$ ablated mice compared with control S1PR1$^{+/+}$ animals ($P < 0.01$; **Figure 6D–F**). ON damage was assessed by performing pNFH immunoreactivity measurements that showed similar changes between Neu-S1PR1$^{-/-}$ ablated mice and S1PR1$^{+/+}$ control mice. However, the siponimod-treated group showed significantly greater immunoreactivity of pNFH only in S1PR1$^{+/+}$ control mice compared with Neu-S1PR1$^{-/-}$ mice ($P < 0.01$; **Additional Figure 4**).

We next analyzed the impact of neuronal S1PR1 ablation on degenerative changes in dLGN of the brain. A significant decline in the frequency of NeuN$^+$ cells was observed in neuronal S1PR1 ablated mice (AAV-GFP-Cre) compared with control S1PR1$^{+/+}$ (AAV-GFP) mice in high IOP conditions ($P < 0.05$). No significant changes in dLGN neuronal cell density were evident in animals subjected to neuronal S1PR1 ablation under normal conditions. Neuronal S1PR1 ablation significantly reduced the protective effects of siponimod on the dLGN degenerative changes. Siponimod treatment showed a significantly greater frequency of NeuN$^+$ cells in S1PR$^{+/+}$ control animals compared with Neu-S1PR1$^{-/-}$ mice ($P < 0.01$) in high IOP conditions (**Figure 7**). Quantitative histological analysis of the neuronal cell density showed a significantly reduced neuronal density ($P < 0.01$) in the dLGN region in Neu-S1PR1$^{-/-}$ ablated mice compared with the control S1PR1$^{+/+}$ animals in high IOP conditions. The protective effect of siponimod on the dLGN neuronal density observed in the control S1PR1$^{+/+}$ mice was significantly diminished in the Neu-S1PR1$^{-/-}$ ablated group under high IOP conditions ($P < 0.01$; **Additional Figure 5**). These results indicated that expression of S1PR1 in the neurons plays a pivotal role in cell survival in the retina and dLGN in high IOP-induced degeneration and that the protective effects of siponimod on the neurons under such conditions are mediated through neuronal S1PR1 expression.

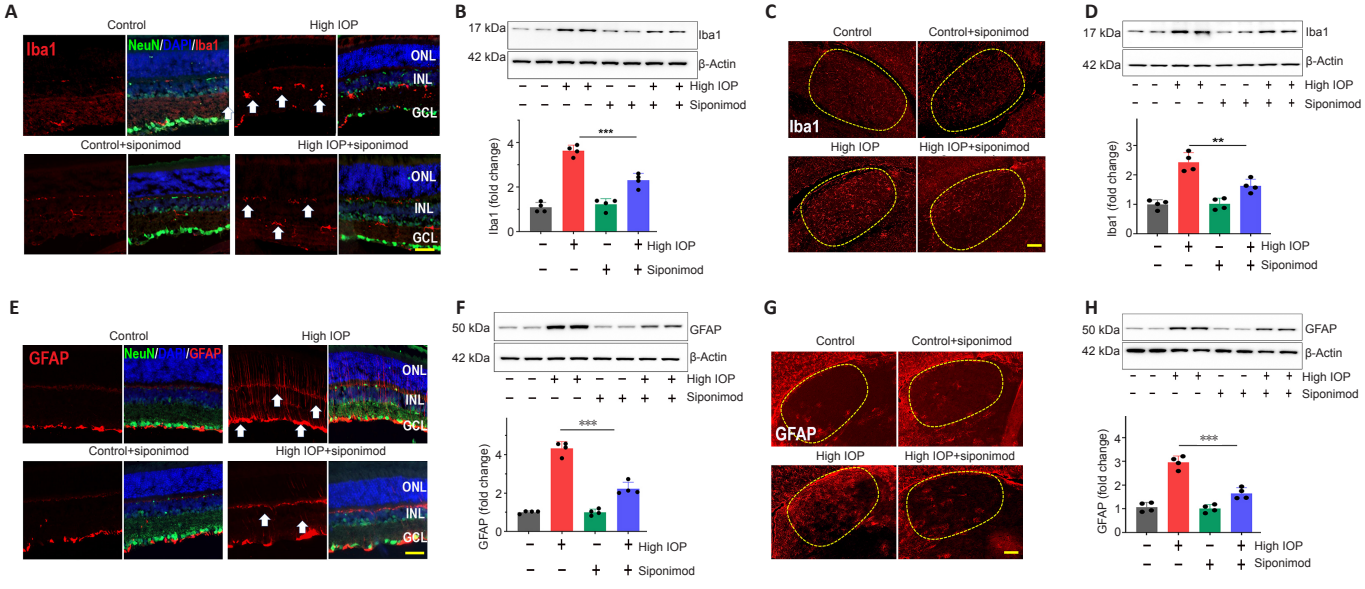

Figure 5 | **Siponimod treatment reduces glial activation along the visual pathway in chronic optic nerve injury condition (8 weeks).**
(A) Immunofluorescence staining of eye sections stained with NeuN, a marker for neurons (green) and Iba1 (red) for microglia (representative images, arrows indicate the changes in expression, scale bar: 50 µm; GCL: ganglion cell layer; INL: inner nuclear layer; ONL: outer nuclear layer). (B) Quantification of Iba1 expression by western blotting analysis of retina lysates (normalized to β-actin). (C) Representative immunofluorescence images of coronal sections of mouse brains (contralateral, the dorsolateral geniculate nucleus (dLGN) is marked with dotted circles, scale bar: 100 µm) stained with Iba1 antibody (red). (D) Western blot analysis of microdissected dLGN and their quantitative analysis for Iba1 expression. (E) Immunofluorescence analysis of reactive gliosis (Muller glia) in the eye sections stained with GFAP (red) (scale bar: 50 µm). (F) Western blot analysis for GFAP expressions in retina lysates and their quantitative analysis. (G) Immunofluorescence staining for brain coronal sections with GFAP (red) (scale bar: 100 µm). (H) Western blot analysis and quantification for GFAP expression in the dLGN. $^{**}P < 0.01$, $^{***}P < 0.001$, one-way analysis of variance with Tukey's multiple comparisons test; $n = 4$ per group. GFAP: Glial fibrillary acidic protein; Iba1: ionized calcium-binding adaptor molecule 1; IOP: intraocular pressure.

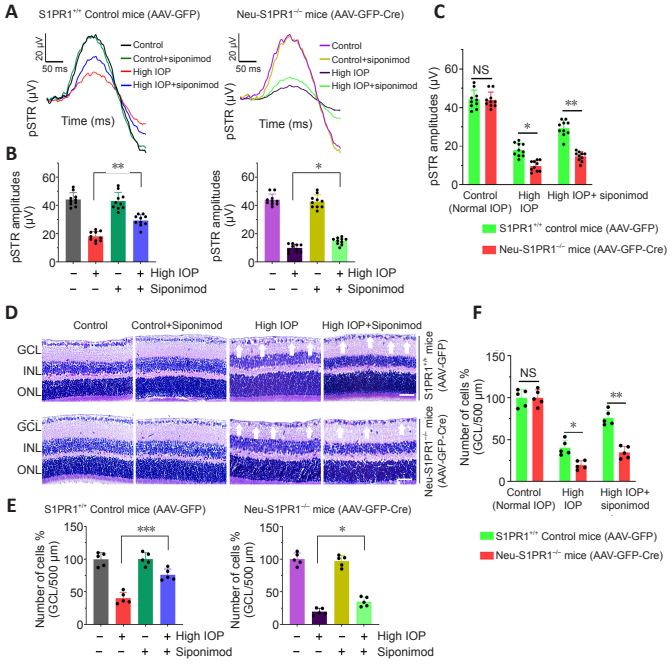

Figure 6 | The functional importance of S1PR1 in neurons and its deletion impairs the protective effect of siponimod on inner retinal function and structure in chronic optic nerve injury condition.

(A) Inner retinal positive scotopic threshold responses (pSTR) responses and (B) quantification of the pSTR amplitudes of control and high intraocular pressure (IOP) eyes (8 weeks) of S1PR1$^{+/+}$ control (AAV-GFP) and Neu-S1PR1$^{-/-}$ (AAV-GFP-Cre) mice groups. (C) Comparison of pSTR amplitudes loss among different mice groups (n = 10 per group). (D) Hematoxylin and eosin staining of eye cross-sections (arrows indicate the changes in cell densities, scale bar: 50 µm. GCL: Ganglion cell layer; INL: inner nuclear layer; ONL: outer nuclear layer) and (E) cell counts in the GCL. (F) Comparison of cell loss in the GCL among different mouse groups (n = 5 per group). *P < 0.05, **P < 0.01, ***P < 0.001, one-way analysis of variance with Tukey's multiple comparisons test. NS: Not significant; S1PR: sphingosine-1-phosphate receptor.

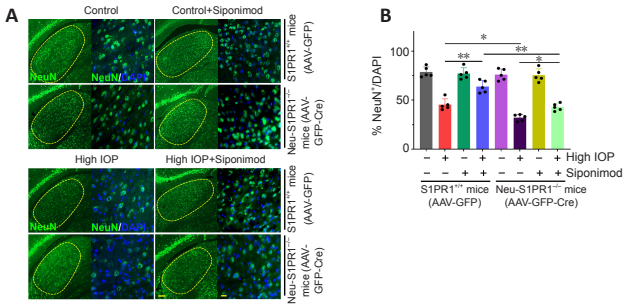

Figure 7 | Neuron-specific deletion of S1PR1 reduced the protective effect of siponimod against trans-neuronal degeneration in dLGN of the brain in chronic optic nerve injury condition.

(A) Representative immunofluorescence images of coronal sections of S1PR1$^{+/+}$ control (AAV-GFP) and Neu-S1PR1$^{-/-}$ (AAV-GFP-Cre) mice brains (contralateral) stained with anti-NeuN (green) and DAPI (blue) (representative, the dLGN is marked with dotted circles, scale bar: 100 µm). (B) Quantification of the percentage of NeuN^{+} cells out of DAPI-positive cells in the dLGN from magnified different areas (scale bar: 20 µm) among mice groups (8 weeks of chronic high IOP). *P < 0.05, **P < 0.01, one-way analysis of variance with Tukey's multiple comparisons test (mean ± SD, n = 5 per group). DAPI: 4′,6-Diamidino-2-phenylindole; AAV: adeno-associated virus; dLGN: dorsolateral geniculate nucleus; IOP: intraocular pressure; S1PR: sphingosine-1-phosphate receptor.

The effect of S1PR1 deletion in neurons on pro-surviving Akt and Erk1/2 pathways was evaluated by Western blot analysis. Mice treated with siponimod showed enhanced Akt and Erk1/2 phosphorylation levels in the retina and dLGN in S1PR$^{+/+}$ control animals (AAV-GFP) in high IOP conditions. S1PR1 ablation in neurons diminished siponimod-induced upregulation of Akt and Erk1/2 phosphorylation. The Neu-S1PR1$^{-/-}$ (AAV-GFP-Cre) mice exhibited significantly decreased Akt and Erk1/2 phosphorylation levels with siponimod treatment both in the retina and dLGN (P < 0.01) in high IOP conditions (**Additional Figure 6**). These results demonstrated that siponimod induces phosphorylation of Akt and Erk1/2 through S1PR1 signaling in neurons.

Protective effects of siponimod on glial activation are attenuated in response to neuronal-specific S1PR1 ablation

We then determined whether the increased degeneration observed in Neu-S1PR1$^{-/-}$ (AAV-GFP-Cre) mice with high IOP might impact siponimod-induced effects on glial activation. Similar to the results described in **Figure 5** and **Additional Figure 1**, hypertrophic activated microglia and reactive gliosis analyzed with Iba1 and GFAP antibodies along the visual pathway were observed in untreated control S1PR1$^{+/+}$ (AAV-GFP) mice in chronic high IOP conditions and this was reduced with siponimod treatment (P < 0.001; **Figure 8** and **Additional Figures 7** and **8**). Western blot quantification revealed a 3.16 ± 0.35-fold increase in Iba1 and 4.30 ± 0.57-fold upregulation of GFAP expression in the retina (P < 0.001) in high IOP conditions compared with the control normal IOP (sham) mice group (**Figure 8C**). Similarly, in the dLGN 2.57 ± 0.28-fold increase for Iba1 and 3.17 ± 0.22-fold increase for GFAP expression were observed with chronic high IOP (P < 0.001; **Additional Figure 7C**). This glial activation was reduced significantly to 1.52 ± 0.18 (dLGN) to 1.69 ± 0.21-fold (retina) for microglia and 2.13 ± 0.27 (dLGN)- to 2.47 ± 0.37-fold (retina) for reactive gliosis with siponimod treatment in S1PR1$^{+/+}$ control mice. This protective effect of siponimod on microglial activation was abolished in Neu-S1PR1$^{-/-}$ mice. However, siponimod treatment showed a significant suppressive effect on reactive gliosis in Neu-S1PR1$^{-/-}$ mice (AAV-GFP-Cre). Siponimod treatment significantly (P < 0.05) reduced GFAP expression from 4.57 ± 0.44 to 3.41 ± 0.35-fold in the retina and 3.72 ± 0.32 to 2.88 ± 0.22-fold in dLGN of the brain in Neu-S1PR1$^{-/-}$ mice under high IOP conditions compared with the untreated mice group. Further, similar levels of effects were observed in ONs evaluated by immunoreactivity of Iba1 and GFAP (**Additional Figure 8**). These results together suggest that a diminished protective effect of siponimod on glia was associated with enhanced degeneration after S1PR1 deletion in neurons.

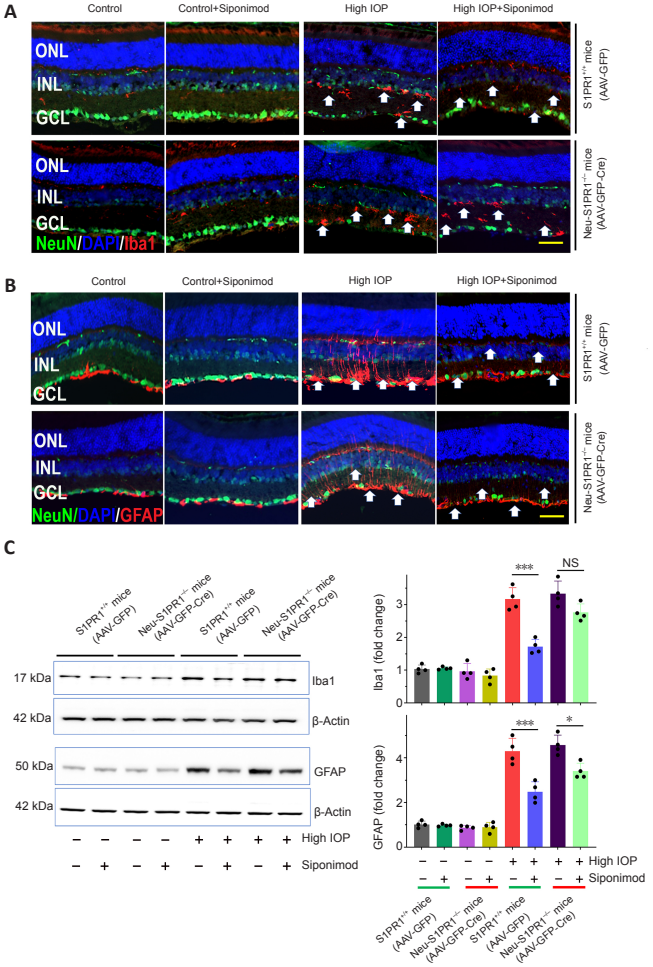

Figure 8 | Attenuation of the protective effect of siponimod on retinal microglial activation and reactive Müller glia in high IOP condition in Neu-S1PR1$^{-/-}$ (AAV-GFP-Cre) mice.

(A) Representative immunofluorescence images of control S1PR1$^{+/+}$ and Neu-S1PR1$^{-/-}$ (AAV-GFP-Cre) mice eyes (8 weeks of chronic high IOP) sections stained with NeuN (green) and Iba1 (red) for microglia and (B) GFAP (red) for Müller glia (arrows indicate the changes in expression, scale bar: 50 µm; GCL: ganglion cell layer; INL: inner nuclear layer; ONL: outer nuclear layer). (C) Western blot analysis and quantification of Iba1 and GFAP expressions in retina lysates (normalized to β actin) (*P < 0.05, ***P < 0.001, n = 4 per group). Statistical significance was determined using one-way analysis of variance with Tukey's multiple comparisons test (mean ± SD). AAV: Adeno-associated virus; GFAP: glial fibrillary acidic protein; Iba1: ionized calcium-binding adaptor molecule 1; IOP: intraocular pressure; NS: not significant; S1PR: sphingosine-1-phosphate receptor.

The protective effects of siponimod are not primarily mediated through S1PR1 expression in oligodendrocytes

Death of oligodendrocytes in elevated IOP conditions has been reported along with axonal loss and RGC degeneration (Nakazawa et al., 2006; Son et al., 2010). Oligodendrocyte-specific S1PR1 deletion in S1PR1$^{flox/flox}$ transgenic mice was achieved using AAV-PHP.eB vector expressing Cre recombinase enzyme under MBP promoter (**Additional Figure 9A**). Successful transduction of the CNS was evaluated by GFP expression on brain sections of the mice injected with AAVs. Immunofluorescence co-staining of the brain sections with GFP and oligodendrocytes specific marker MBP revealed the localization of GFP signal with MBP expression (**Additional Figure 9B** and **C**), indicating AAVs' transduction in oligodendrocytes. Transduction efficiency assessed by measurement of GFP$^+$ area to total MBP revealed 77.56 ± 5.53% for GFP control and 76.56 ± 5.43% Cre recombinase AAVs in dLGN of the brain (**Additional Figure 9D**). Western blot analysis of brain tissue (dLGN) revealed GFP expression in mice injected with AAVs. Densitometric quantification demonstrated the S1PR1 expression was decreased by 32.68 ± 6.57% in the brain in AAV-Cre injected mice (**Additional Figure 9E** and **F**).

The control S1PR$^{+/+}$ (AAV-GFP) mice and oligodendrocyte-specific S1PR1$^{-/-}$ (Oligo-S1PR1$^{-/-}$, AAV-GFP-Cre) mice eyes experienced similar levels of IOP increase (20–23 mmHg) (**Additional Figure 10**). Deletion of S1PR1 in oligodendrocytes did not display any significant effects on retinal structure and function of the retina in ON injury conditions. Similar levels of pSTR amplitude losses were observed between control and Oligo-S1PR1$^{-/-}$ (AAV-GFP-Cre) mice groups (18.67 ± 5.93 μV *vs*. 17.89 ± 4.76 μV) in high IOP conditions compared with the control normal IOP (sham) mice (P < 0.001; **Additional Figure 11A** and **B**). Further, deletion of S1PR1 in oligodendrocytes did not change the protective effects of siponimod, with a similar level of protection of 63.63 ± 4.93% and 60.29 ± 5.59% against pSTR amplitudes loss was observed in control and Oligo-S1PR1$^{-/-}$ (AAV-GFP-Cre) mice groups, respectively, compared with the untreated mice group (P < 0.01). Cell counts in the GCL further supported the above effects and showed a similar extent of cell losses (60.23 ± 10.18% *vs*. 61.15 ± 10.9%). Siponimod treatment showed no significant differences in the protection conferred by drug treatment in both control and Oligo-S1PR1$^{-/-}$ mice groups (GCL density: 77.8 ± 9.2% *vs*. 74.22 ± 10.11%) in glaucomatous injury compared with the untreated mice group (P < 0.001; **Additional Figure 11C** and **D**).

The extent of ON damage as assessed by pNFH immunofluorescence staining revealed similar levels of decrease in pNFH immunoreactivity between Oligo-S1PR1$^{-/-}$ ablated mice (AV-GFP-Cre) and S1PR1$^{+/+}$ (AAV-GFP) control mice (66.53 ± 9.85% *vs.* 66.0 ± 9.01%) in high IOP conditions compared with the control normal IOP (sham) mice (P < 0.001). Siponimod treatment also showed similar levels of protective effect between control and Oligo-S1PR1$^{-/-}$ mice groups in ON injury (63.86 ± 8.02% *vs*. 63.93 ± 8.84%) compared with the untreated mice group (P < 0.01; **Additional Figure 12A** and **B**). Further, the ablation of S1PR1 in oligodendrocytes did not impact the degenerative changes in the dLGN. NeuN$^+$ cell density in dLGN did not change significantly in Oglio-S1PR1$^{-/-}$ ablated mice compared with control S1PR1$^{+/+}$ mice (39.17 ± 6.10% *vs.* 42.8 ± 7.26%) in elevated IOP compared with the normal IOP conditions (P < 0.01). Similarly, siponimod treatment did not exhibit any significant differences in the degenerative changes in the dLGN (**Additional Figure 12C** and **D**). These results suggest that high IOP-induced degenerative changes in the dLGN were not primarily mediated through S1PR1 expression in oligodendrocytes and that the protective effects of siponimod are not mediated through oligodendrocyte-specific S1PR1 expression.

Discussion

This study demonstrates that siponimod treatment protects the retina and higher visual pathway in the ON injury model. We further examined the impact of S1PR1 deletion in neurons and oligodendrocytes using cell-specific conditional S1PR1 ablated mice. Siponimod treatment was recently demonstrated to reduce disability progression in a clinical trial involving secondary progressive MS patients (Gajofatto, 2017; Dumitrescu et al., 2019). This suggested that siponimod might have neuroprotective potential as the progressive form of MS is a chronic condition mainly driven by local CNS degenerative mechanisms (Frohman et al., 2005; Baecher-Allan et al., 2018). In this study, our results revealed that siponimod mediates neuroprotective effects on the retina and dLGN of the brain through neuronal S1PR1 in ON injury conditions and is independent of peripheral immunomodulatory effects.

S1PR1 modulation by S1P or FTY720 has been associated with mitogenic and pro-survival actions in neurons *in vivo* and *in vitro* through activation of Akt and Erk pathways (Ye et al., 2016; Zhao et al., 2017; Motyl et al., 2018). We observed reduced Akt and Erk 1/2 phosphorylation levels in the retina and dLGN in glaucomatous injury conditions, and these pathways were upregulated following siponimod administration. Further, we identified that deletion of S1PR1 in neurons reduced the siponimod-induced activation of Akt and Erk 1/2. These results suggest that neuroprotective actions of siponimod are determined by activation of pro-survival Akt and Erk 1/2 kinase signaling through S1PR1 in neurons. Previously, activation of Akt and Erk 1/2 signaling by FTY720 treatment has been shown to be anti-apoptotic and neuroprotective in neuronal cultures as well as in rodent models of stroke (Hasegawa et al., 2010), traumatic brain injury (Ye et al., 2016), and Parkinson's disease (Zhao et al., 2017; Zhang and Wang, 2020).

Microglia and astrocytes in the brain and Müller glial cells in the retina are the primary resident innate immune components, and their activation has been associated with glaucomatous neuronal injury (Mélik Parsadaniantz et al., 2020; Rolle et al., 2020). We observed glial cell activation in terms of morphological changes, proliferation, and upregulation of GFAP in reactive Müller glia and astroglia along the visual pathway in response to high IOP. This activation was significantly reduced in siponimod-treated mice, as confirmed with western blot and immunofluorescence analysis of retina, ON, and the brain tissues. The S1PRs expressed in astrocytes and microglia are also targets of siponimod and fingolimod, and their modulation has been reported to be neuroprotective (Noda et al., 2013; Qin et al., 2017; Rothhammer et al., 2017; Colombo et al., 2020). Further investigations into the specific inflammatory pathways affected in response to tissue-resident glial cell modulation by siponimod will unravel their roles in providing neuroprotective effects in chronic glaucoma.

Our study also demonstrates that S1PR1 expression in RGCs in the retina and neuronal cells in the dLGN is crucial to their survival in ON injury conditions. S1PR1 is expressed in sensory, dopaminergic, cortical, hypothalamic POMC neurons, and RGCs (Silva et al., 2014; Joly and Pernet, 2016; Ye et al., 2016; Zhao et al., 2017), and its deletion was observed to be embryonically lethal (Mizugishi et al., 2005). Therefore, we generated neuron-specific S1PR1 ablation *in vivo* in S1PR1$^{flox/flox}$ adult mice using engineered AAV-Cre recombinase constructs that efficiently transduced the neuronal cells or oligodendrocytes (Chan et al., 2017). In normal conditions, the neuronal deletion of S1PR1 did not significantly affect the inner retinal structure, function, and dLGN neuronal density. However, with glaucomatous injury, enhanced degenerative changes occurred in the inner retina and dLGN. These results suggested that the neuronal S1PR1 is necessary for neuroprotection against ON injury, but maybe not for their maintenance. Further, the protective effects of siponimod were impaired significantly in Neu-S1PR1$^{-/-}$ mice. Among all S1P receptors, S1PR1 is a unique G-protein-coupled receptor, exclusively coupled with a Gi protein and has been linked to neuroprotection mechanism in neurons in different neurogenerative conditions, including stroke, traumatic brain injury, and Parkinson's disease (Ye et al., 2016; Zhao et al., 2017; Lucaciu et al., 2020). S1PR1 signal is transduced through Akt, Erk/MAP kinase pathways, and the S1PR1/STAT3 axis, promoting cell survival, proliferation, differentiation, and energy homeostasis (Pyne and Pyne, 2017). Activation of Jak2/STAT3 through the glycoprotein 130 receptor-dependent or independent mechanisms also promotes axon regeneration and neuronal survival effects (Smith et al., 2009; Nicolas et al., 2013). S1PR1 is a critical regulator of neurogenesis and neuronal cell apoptosis during development, and its deletion increased embryonic neuronal apoptosis (Mizugishi et al., 2005). Our results in this study suggest that S1PR1 is required for neuronal survival activity during ON injury conditions.

Neuronal-specific S1PR1 deletion was observed to exacerbate the retinal and dLGN deficits and resulted in reduced efficacy of siponimod on activated glial cells. This could be due to the neuronal damage-triggering an enhanced inflammatory burst by upregulating the purinergic receptor responses in microglia. Extracellular nucleotides released by damaged neurons are reported to upregulate purinergic receptors of microglia and activate their inflammatory response, migration, and phagocytic ability (Illes et al., 2020; Pietrowski et al., 2021). We observed significantly reduced reactive gliosis in Neu-S1PR1$^{-/-}$ mice with siponimod treatment in the retina, ON, and dLGN. These results suggest that the protective effects of siponimod in neuronal S1PR1 deleted mice might be through suppression of reactive gliosis in the retina and the brain. Suppression of pathogenic activation of astrocytes by S1PR1 modulation has previously been observed in various CNS inflammatory conditions (Chatzikonstantinou et al., 2021). Modulation of S1PR by either FTY720 or siponimod has been shown to suppress astrocytic activation. FTY720 treatment downregulated the expression of proinflammatory, chemoattractant, and neurotoxic molecules by activated astrocytes and microglia and enhanced the neuroprotective molecules like Cxcl12, IL33 Csf2, Chi3l3, and IL10 in the CNS in MS animal model (Choi et al., 2011; Rothhammer et al., 2017). S1PR agonist treatment has been shown to reduce the inflammatory response of astrocytes by reducing pro-inflammatory cytokines production, hampering the NFkB pathway, and blockage of nitric oxide (Miguez et al., 2015; Colombo et al., 2020; Kipp, 2020).

In addition, we evaluated whether the oligodendrocyte-specific deletion of S1PR1 has any effect on retinal and dLGN degeneration in experimental glaucoma and whether siponimod treatment imparted protective effects under such conditions. Oligodendrolineage cells express S1PR1 predominately, together with S1PR2 and S1PR5, and their expression levels vary during the maturation stage. Oligodendrocyte precursor cells preferentially express S1PR1, and its level decreases during differentiation, and S1PR5 becomes the dominant subtype in mature oligodendrocytes (Healy and Antel, 2016; Roggeri et al., 2020). In our study oligodendrocyte-specific S1PR1 deletion resulted in degenerative changes in the retina and dLGN similar to wt/control mice, and siponimod treatment also did not alter the neuroprotective effects in high IOP conditions, suggesting that the protective effects of the drug are not mediated through oligodendrocyte S1PR1 expression. However, S1PR signaling alteration is suggested to play distinct pathophysiological roles and displays specific subtype activation in neurodegenerative processes. S1PR1 ablated oligodendrocytes were previously shown to be more susceptible to demyelinating agents (Roggeri et al., 2020).

Small size pharmacological derivatives have been developed that can be applied topically on the corneal surface or administered systemically. While

topical ocular drug installation through drops or ointment is a convenient and widely preferred route of drug administration, physiological barriers reduce the penetration of drugs to the posterior segment (Edelhauser et al., 2010). Various novel drug delivery strategies such as emulsions, liposomes, nano-micelles, and nanoparticles have been developed to surpass these barriers and enhance drug levels in tissues (Amadio et al., 2016; Kang-Mieler et al., 2020; Kim and Woo, 2021). In this regard, using an innovative ocular drug delivery system like nanoencapsulation could enhance siponimod delivery to the retina and facilitate its topical administration in the future.

This study has some limitations that may require further investigations. In our findings, the mice treated with a single dose of siponimod via diet (10 mg/kg diet) showed significant neuroprotection against glaucomatous injury on the visual pathway. Further studies are required to understand the different dose effects of siponimod. We observed significant downregulation of glial activation with siponimod treatment in high IOP conditions both in the retina and the brain. However, we have not analyzed the inflammatory pathways affected by the siponimod treatment. S1PR1 is also expressed by the glial cells. Therefore, further investigations into the glial responses to siponimod treatment are required to understand the neuroprotective effects of siponimod in chronic glaucoma. Additionally, our study revealed that neuronal S1PR1 plays a critical role in glaucomatous injury, but we have not followed the long-term effects of its deletion in normal conditions. Despite these few limitations of this study, our findings suggest that modulation of neuronal S1PR1 by siponimod treatment could be beneficial in providing neuroprotection against glaucoma injury.

In summary, our results demonstrated that siponimod exerts neuroprotective effects on the retina and the brain in an ON-injury model. S1PR1 signaling in neurons plays a crucial role in neuroprotection and induces Akt/Erk pathways activation. Furthermore, this study showed that siponimod exerts beneficial effects through S1PR1 in neurons. The drug exhibited suppressive effects on the microglial activation and reactive gliosis along with neuronal cell preservation. Therefore, this study identifies that modulation of S1P receptors within the CNS may offer promising strategies to provide neuroprotection in CNS injury conditions.

Author contributions: *DB, VG, MM, AK and SLG designed the study; DB, RVW, NC, KP, and RR performed the experiments; DB, VG, and SLG analyzed the data; DB and VG wrote the manuscript; MM, SS helped to write the manuscript. All authors helped to write the manuscript preparation and approved the final version of the manuscript.*

Conflicts of interest: *The authors declare that they have no competing interests. No conflicts of interest exist between Novartis and publication of this paper.*

Availability of data and materials: *The authors declare that all the relevant data, associated protocols, and materials supporting the findings of this study are present in the paper and/or the Additional Materials.*

Additional files:

Additional Figure 1: *Siponimod treatment reduced glial activation in optic nerves in chronic high IOP (8 weeks) condition.*

Additional Figure 2: *Neuronal specific deletion of S1PR1 using AAV-PHP.eB-Syn1-GFP-Cre in S1PR1$^{flox/flox}$ transgenic mice.*

Additional Figure 3: *Chronic IOP elevation in different group mice eyes for 8 weeks following microbead injections.*

Additional Figure 4: *Effects of siponimod on optic nerve damage under optic nerve injury induced by high IOP (8 weeks) in control and Neu-S1PR1$^{-/-}$ (AAV-GFP-Cre) mice groups.*

Additional Figure 5: *Effects of neuronal-specific S1PR1 deletion on dLGN degenerative changes under chronic IOP condition (8 weeks).*

Additional Figure 6: *Deletion of S1PR1 in neurons reduces siponimod mediated upregulation of pro-survival signaling pathways Akt and Erk1/2 in the retina and brain.*

Additional Figure 7: *Siponimod suppresses microglial activation and reactive astrocytes in dLGN in control mice and its protective effect is reduced in Neu-S1PR1$^{-/-}$ (AAV-GFP-Cre) mice in chronic optic nerve injury condition.*

Additional Figure 8: *Effects of siponimod on glial activation in optic nerve under high IOP (8 weeks) induced optic nerve injury.*

Additional Figure 9: *Transduction and specific deletion of S1PR1 in oligodendrocytes using AAV-PHP.eB-MBP-GFP-Cre in S1PR1$^{flox/flox}$ transgenic mice.*

Additional Figure 10: *Chronic IOP elevation in different group mice eyes for 8 weeks following microbead injections.*

Additional Figure 11: *Effects of oligodendrocyte-specific S1PR1 deletion on retinal degenerative changes under chronic IOP condition.*

Additional Figure 12: *Effects of oligodendrocyte-specific deletion of S1PR1 on optic nerve and dLGN neurodegeneration under high IOP (8 weeks) optic nerve injury condition.*

References

Abbasi M, Gupta VK, Chitranshi N, Gupta VB, Mirzaei M, Dheer Y, Garthwaite L, Zaw T, Parton RG, You Y, Graham SL (2020) Caveolin-1 ablation imparts partial protection against inner retinal injury in experimental glaucoma and reduces apoptotic activation. Mol Neurobiol 57:3759-3784.

Abbasi M, Gupta VK, Chitranshi N, Gupta V, Ranjbaran R, Rajput R, Pushpitha K, Kb D, You Y, Salekdeh GH, Parton RG, Mirzaei M, Graham SL (2021) Inner retinal injury in experimental glaucoma is prevented upon AAV mediated Shp2 silencing in a caveolin dependent manner. Theranostics 11:6154-6172.

Amadio M, Pascale A, Cupri S, Pignatello R, Osera C, D Agata V, D Amico AG, Leggio GM, Ruozi B, Govoni S, Drago F, Bucolo C (2016) Nanosystems based on siRNA silencing HuR expression counteract diabetic retinopathy in rat. Pharmacol Res 111:713-720.

Artero-Castro A, Rodriguez-Jimenez FJ, Jendelova P, VanderWall KB, Meyer JS, Erceg S (2020) Glaucoma as a neurodegenerative disease caused by intrinsic vulnerability factors. Prog Neurobiol 193:101817.

Baecher-Allan C, Kaskow BJ, Weiner HL (2018) Multiple sclerosis: mechanisms and immunotherapy. Neuron 97:742-768.

Behrangi N, Fischbach F, Kipp M (2019) Mechanism of siponimod: anti-inflammatory and neuroprotective mode of action. Cells 8:24.

Bertacchi M, Gruart A, Kaimakis P, Allet C, Serra L, Giacobini P, Delgado-García JM, Bovolenta P, Studer M (2019) Mouse Nr2f1 haploinsufficiency unveils new pathological mechanisms of a human optic atrophy syndrome. EMBO Mol Med 11:e10291.

Bigaud M, Rudolph B, Briard E, Beerli C, Hofmann A, Hermes E, Muellershausen F, Schubart A, Gardin A (2021) Siponimod (BAF312) penetrates, distributes, and acts in the central nervous system: Preclinical insights. Mult Scler J Exp Transl Clin 7:20552173211049168.

Cartier A, Hla T (2019) Sphingosine 1-phosphate: Lipid signaling in pathology and therapy. Science 366:eaar5551.

Chan KY, Jang MJ, Yoo BB, Greenbaum A, Ravi N, Wu WL, Sánchez-Guardado L, Lois C, Mazmanian SK, Deverman BE, Gradinaru V (2017) Engineered AAVs for efficient noninvasive gene delivery to the central and peripheral nervous systems. Nat Neurosci 20:1172-1179.

Chatzikonstantinou S, Poulidou V, Arnaoutoglou M, Kazis D, Heliopoulos I, Grigoriadis N, Boziki M (2021) Signaling through the S1P-S1PR axis in the gut, the immune and the central nervous system in multiple sclerosis: implication for pathogenesis and treatment. Cells 10:3217.

Chidlow G, Ebneter A, Wood JP, Casson RJ (2011) The optic nerve head is the site of axonal transport disruption, axonal cytoskeleton damage and putative axonal regeneration failure in a rat model of glaucoma. Acta Neuropathol 121:737-751.

Chitranshi N, Dheer Y, Mirzaei M, Wu Y, Salekdeh GH, Abbasi M, Gupta V, Vander Wall R, You Y, Graham SL, Gupta V (2019) Loss of Shp2 rescues BDNF/TrkB signaling and contributes to improved retinal ganglion cell neuroprotection. Mol Ther 27:424-441.

Choi JW, Gardell SE, Herr DR, Rivera R, Lee CW, Noguchi K, Teo ST, Yung YC, Lu M, Kennedy G, Chun J (2011) FTY720 (fingolimod) efficacy in an animal model of multiple sclerosis requires astrocyte sphingosine 1-phosphate receptor 1 (S1P1) modulation. Proc Natl Acad Sci U S A 108:751-756.

Chun J, Kihara Y, Jonnalagadda D, Blaho VA (2019) Fingolimod: lessons learned and new opportunities for treating multiple sclerosis and other disorders. Annu Rev Pharmacol Toxicol 59:149-170.

Colombo E, Bassani C, De Angelis A, Ruffini F, Ottoboni L, Comi G, Martino G, Farina C (2020) Siponimod (BAF312) activates Nrf2 while hampering NFκB in human astrocytes, and protects from astrocyte-induced neurodegeneration. Front Immunol 11:635.

Dheer Y, Chitranshi N, Gupta V, Sharma S, Pushpitha K, Abbasi M, Mirzaei M, You Y, Graham SL, Gupta V (2019) Retinoid x receptor modulation protects against ER stress response and rescues glaucoma phenotypes in adult mice. Exp Neurol 314:111-125.

Dietrich M, Hecker C, Beerli C, Moebs C, Ramseier P, Afatsawo C, Bigaud M, Albrecht P (2018) Optimising Siponimod (BAF312) oral administration for long-term experimental studies in mice. In: Multiple sclerosis journal, pp 913-914. London: Sage Publications Ltd.

Dumitrescu L, Constantinescu CS, Tanasescu R (2019) Siponimod for the treatment of secondary progressive multiple sclerosis. Expert Opin Pharmacother 20:143-150.

Edelhauser HF, Rowe-Rendleman CL, Robinson MR, Dawson DG, Chader GJ, Grossniklaus HE, Rittenhouse KD, Wilson CG, Weber DA, Kuppermann BD, Csaky KG, Olsen TW, Kompella UB, Holers VM, Hageman GS, Gilger BC, Campochiaro PA, Whitcup SM, Wong WT (2010) Ophthalmic drug delivery systems for the treatment of retinal diseases: basic research to clinical applications. Invest Ophthalmol Vis Sci 51:5403-5420.

Frohman EM, Filippi M, Stuve O, Waxman SG, Corboy J, Phillips JT, Lucchinetti C, Wilken J, Karandikar N, Hemmer B, Monson N, De Keyser J, Hartung H, Steinman L, Oksenberg JR, Cree BA, Hauser S, Racke MK (2005) Characterizing the mechanisms of progression in multiple sclerosis: evidence and new hypotheses for future directions. Arch Neurol 62:1345-1356.

Gajofatto A (2017) Spotlight on siponimod and its potential in the treatment of secondary progressive multiple sclerosis: the evidence to date. Drug Des Devel Ther 11:3153-3157.
Gupta N, Ly T, Zhang Q, Kaufman PL, Weinreb RN, Yücel YH (2007) Chronic ocular hypertension induces dendrite pathology in the lateral geniculate nucleus of the brain. Exp Eye Res 84:176-184.
Gupta VK, You Y, Klistorner A, Graham SL (2012) Focus on molecules: sphingosine 1 phosphate (S1P). Exp Eye Res 103:119-120.
Hasegawa Y, Suzuki H, Sozen T, Rolland W, Zhang JH (2010) Activation of sphingosine 1-phosphate receptor-1 by FTY720 is neuroprotective after ischemic stroke in rats. Stroke 41:368-374.
Healy LM, Antel JP (2016) Sphingosine-1-phosphate receptors in the central nervous and immune systems. Curr Drug Targets 17:1841-1850.
Hunter SF, Bowen JD, Reder AT (2016) The direct effects of fingolimod in the central nervous system: implications for relapsing multiple sclerosis. CNS Drugs 30:135-147.
Illes P, Rubini P, Ulrich H, Zhao Y, Tang Y (2020) Regulation of microglial functions by purinergic mechanisms in the healthy and diseased CNS. Cells 9:1108.
Joly S, Pernet V (2016) Sphingosine 1-phosphate receptor 1 is required for retinal ganglion cell survival after optic nerve trauma. J Neurochem 138:571-586.
Joly S, Lamoureux S, Pernet V (2017) Nonamyloidogenic processing of amyloid beta precursor protein is associated with retinal function improvement in aging male APP(swe)/PS1ΔE9 mice. Neurobiol Aging 53:181-191.
Jonas JB, Aung T, Bourne RR, Bron AM, Ritch R, Panda-Jonas S (2017) Glaucoma. Lancet 390:2183-2193.
Kang-Mieler JJ, Rudeen KM, Liu W, Mieler WF (2020) Advances in ocular drug delivery systems. Eye (Lond) 34:1371-1379.
Kappos L, Antel J, Comi G, Montalban X, O'connor P, Polman CH, Haas T, Korn AA, Karlsson G, Radue EW (2006) Oral fingolimod (FTY720) for relapsing multiple sclerosis. N Engl J Med 355:1124-1140.
Kappos L, Bar-Or A, Cree BAC, Fox RJ, Giovannoni G, Gold R, Vermersch P, Arnold DL, Arnould S, Scherz T, Wolf C, Wallström E, Dahlke F (2018) Siponimod versus placebo in secondary progressive multiple sclerosis (EXPAND): a double-blind, randomised, phase 3 study. Lancet 391:1263-1273.
Karunakaran I, van Echten-Deckert G (2017) Sphingosine 1-phosphate-A double edged sword in the brain. Biochim Biophys Acta Biomembr 1859:1573-1582.
Kashiwagi K, Ou B, Nakamura S, Tanaka Y, Suzuki M, Tsukahara S (2003) Increase in dephosphorylation of the heavy neurofilament subunit in the monkey chronic glaucoma model. Invest Ophthalmol Vis Sci 44:154-159.
Kim HM, Woo SJ (2021) Ocular drug delivery to the retina: current innovations and future perspectives. Pharmaceutics 13:108.
Kipp M (2020) Does siponimod exert direct effects in the central nervous system? Cells 9:1771.
London A, Benhar I, Schwartz M (2013) The retina as a window to the brain-from eye research to CNS disorders. Nat Rev Neurol 9:44-53.
Lucaciu A, Brunkhorst R, Pfeilschifter JM, Pfeilschifter W, Subburayalu J (2020) The S1P-S1PR axis in neurological disorders-insights into current and future therapeutic perspectives. Cells 9(6):1515.
Martin R, Sospedra M (2014) Sphingosine-1 phosphate and central nervous system. Curr Top Microbiol Immunol 378:149-170.
Mélik Parsadaniantz S, Réaux-le Goazigo A, Sapienza A, Habas C, Baudouin C (2020) Glaucoma: A degenerative optic neuropathy related to neuroinflammation? Cells 9:535.
Miguez A, García-Díaz Barriga G, Brito V, Straccia M, Giralt A, Ginés S, Canals JM, Alberch J (2015) Fingolimod (FTY720) enhances hippocampal synaptic plasticity and memory in Huntington's disease by preventing p75NTR up-regulation and astrocyte-mediated inflammation. Hum Mol Genet 24:4958-4970.
Mirzaei M, Gupta VK, Chitranshi N, Deng L, Pushpitha K, Abbasi M, Chick JM, Rajput R, Wu Y, McKay MJ, Salekdeh GH, Gupta VB, Haynes PA, Graham SL (2020) Retinal proteomics of experimental glaucoma model reveal intraocular pressure-induced mediators of neurodegenerative changes. J Cell Biochem doi: 10.1002/jcb.29822.
Mizugishi K, Yamashita T, Olivera A, Miller GF, Spiegel S, Proia RL (2005) Essential role for sphingosine kinases in neural and vascular development. Mol Cell Biol 25:11113-11121.
Motyl J, Przykaza Ł, Boguszewski PM, Kosson P, Strosznajder JB (2018) Pramipexole and Fingolimod exert neuroprotection in a mouse model of Parkinson's disease by activation of sphingosine kinase 1 and Akt kinase. Neuropharmacology 135:139-150.
Nakazawa T, Nakazawa C, Matsubara A, Noda K, Hisatomi T, She H, Michaud N, Hafezi-Moghadam A, Miller JW, Benowitz LI (2006) Tumor necrosis factor-α mediates oligodendrocyte death and delayed retinal ganglion cell loss in a mouse model of glaucoma. J Neurosci 26:12633-12641.
Nicolas CS, Amici M, Bortolotto ZA, Doherty A, Csaba Z, Fafouri A, Dournaud P, Gressens P, Collingridge GL, Peineau S (2013) The role of JAK-STAT signaling within the CNS. JAKSTAT 2:e22925.
Noda H, Takeuchi H, Mizuno T, Suzumura A (2013) Fingolimod phosphate promotes the neuroprotective effects of microglia. J Neuroimmunol 256:13-18.
O'Sullivan S, Dev KK (2017) Sphingosine-1-phosphate receptor therapies: advances in clinical trials for CNS-related diseases. Neuropharmacology 113:597-607.
Pang IH, Clark AF (2020) Inducible rodent models of glaucoma. Prog Retin Eye Res 75:100799.
Pietrowski MJ, Gabr AA, Kozlov S, Blum D, Halle A, Carvalho K (2021) Glial purinergic signaling in neurodegeneration. Front Neurol 12:654850.
Pyne NJ, Pyne S (2017) Sphingosine 1-phosphate receptor 1 signaling in mammalian cells. Molecules 22:344.
Qin C, Fan W-H, Liu Q, Shang K, Murugan M, Wu LJ, Wang W, Tian DS (2017) Fingolimod protects against ischemic white matter damage by modulating microglia toward M2 polarization via STAT3 pathway. Stroke 48:3336-3346.
Rai SN, Dilnashin H, Birla H, Singh SS, Zahra W, Rathore AS, Singh BK, Singh SP (2019) The role of PI3K/Akt and ERK in neurodegenerative disorders. Neurotox Res 35:775-795.
Rodriguez L, Mdzomba JB, Joly S, Boudreau-Laprise M, Planel E, Pernet V (2018) Human tau expression does not induce mouse retina neurodegeneration, suggesting differential toxicity of tau in brain vs. retinal neurons. Front Mol Neurosci 11:293.
Roggeri A, Schepers M, Tiane A, Rombaut B, van Veggel L, Hellings N, Prickaerts J, Pittaluga A, Vanmierlo T (2020) Sphingosine-1-phosphate receptor modulators and oligodendroglial cells: beyond immunomodulation. Int J Mol Sci 21:7537.
Rolle T, Ponzetto A, Malinverni L (2020) The role of neuroinflammation in glaucoma: an update on molecular mechanisms and new therapeutic options. Front Neurol 11:612422.
Rothhammer V, Kenison JE, Tjon E, Takenaka MC, de Lima KA, Borucki DM, Chao CC, Wilz A, Blain M, Healy L, Antel J, Quintana FJ (2017) Sphingosine 1-phosphate receptor modulation suppresses pathogenic astrocyte activation and chronic progressive CNS inflammation. Proc Natl Acad Sci U S A 114:2012-2017.
Schneider CA, Rasband WS, Eliceiri KW (2012) NIH Image to ImageJ: 25 years of image analysis. Nat Methods 9:671-675.
Silva VR, Micheletti TO, Pimentel GD, Katashima CK, Lenhare L, Morari J, Mendes MC, Razolli DS, Rocha GZ, de Souza CT, Ryu D, Prada PO, Velloso LA, Carvalheira JB, Pauli JR, Cintra DE, Ropelle ER (2014) Hypothalamic S1P/S1PR1 axis controls energy homeostasis. Nat Commun 5:4859.
Simkins TJ, Duncan GJ, Bourdette D (2021) Chronic demyelination and axonal degeneration in multiple sclerosis: pathogenesis and therapeutic implications. Curr Neurol Neurosci Rep 21:26.
Smith PD, Sun F, Park KK, Cai B, Wang C, Kuwako K, Martinez-Carrasco I, Connolly L, He Z (2009) SOCS3 deletion promotes optic nerve regeneration in vivo. Neuron 64:617-623.
Son JL, Soto I, Oglesby E, Lopez-Roca T, Pease ME, Quigley HA, Marsh-Armstrong N (2010) Glaucomatous optic nerve injury involves early astrocyte reactivity and late oligodendrocyte loss. Glia 58:780-789.
Sriram P, Graham SL, Wang C, Yiannikas C, Garrick R, Klistorner A (2012) Transsynaptic retinal degeneration in optic neuropathies: optical coherence tomography study. Invest Ophthalmol Vis Sci 53:1271-1275.
Xu F, Na L, Li Y, Chen L (2020) Roles of the PI3K/AKT/mTOR signalling pathways in neurodegenerative diseases and tumours. Cell Biosci 10:54.
Ye Y, Zhao Z, Xu H, Zhang X, Su X, Yang Y, Yu X, He X (2016) Activation of sphingosine 1-phosphate receptor 1 enhances hippocampus neurogenesis in a rat model of traumatic brain injury: an involvement of MEK/Erk signaling pathway. Neural Plast 2016:8072156.
You Y, Gupta VK, Li JC, Klistorner A, Graham SL (2013) Optic neuropathies: characteristic features and mechanisms of retinal ganglion cell loss. Rev Neurosci 24:301-321.
You Y, Gupta VK, Li JC, Al-Adawy N, Klistorner A, Graham SL (2014) FTY720 protects retinal ganglion cells in experimental glaucoma. Invest Ophthalmol Vis Sci 55:3060-3066.
You Y, Joseph C, Wang C, Gupta V, Liu S, Yiannikas C, Chua BE, Chitranshi N, Shen T, Dheer Y, Invernizzi A, Borotkanics R, Barnett M, Graham SL, Klistorner A (2019) Demyelination precedes axonal loss in the transneuronal spread of human neurodegenerative disease. Brain 142:426-442.
Yücel Y, Gupta N (2008) Glaucoma of the brain: a disease model for the study of transsynaptic neural degeneration. Prog Brain Res 173:465-478.
Zhang L, Wang H (2020) FTY720 in CNS injuries: Molecular mechanisms and therapeutic potential. Brain Res Bull 164:75-82.
Zhao P, Yang X, Yang L, Li M, Wood K, Liu Q, Zhu X (2017) Neuroprotective effects of fingolimod in mouse models of Parkinson's disease. FASEB J 31:172-179.

C-Editor: Zhao M; S-Editor: Li CH; L-Editors: Li CH, Song LP; T-Editor: Jia Y

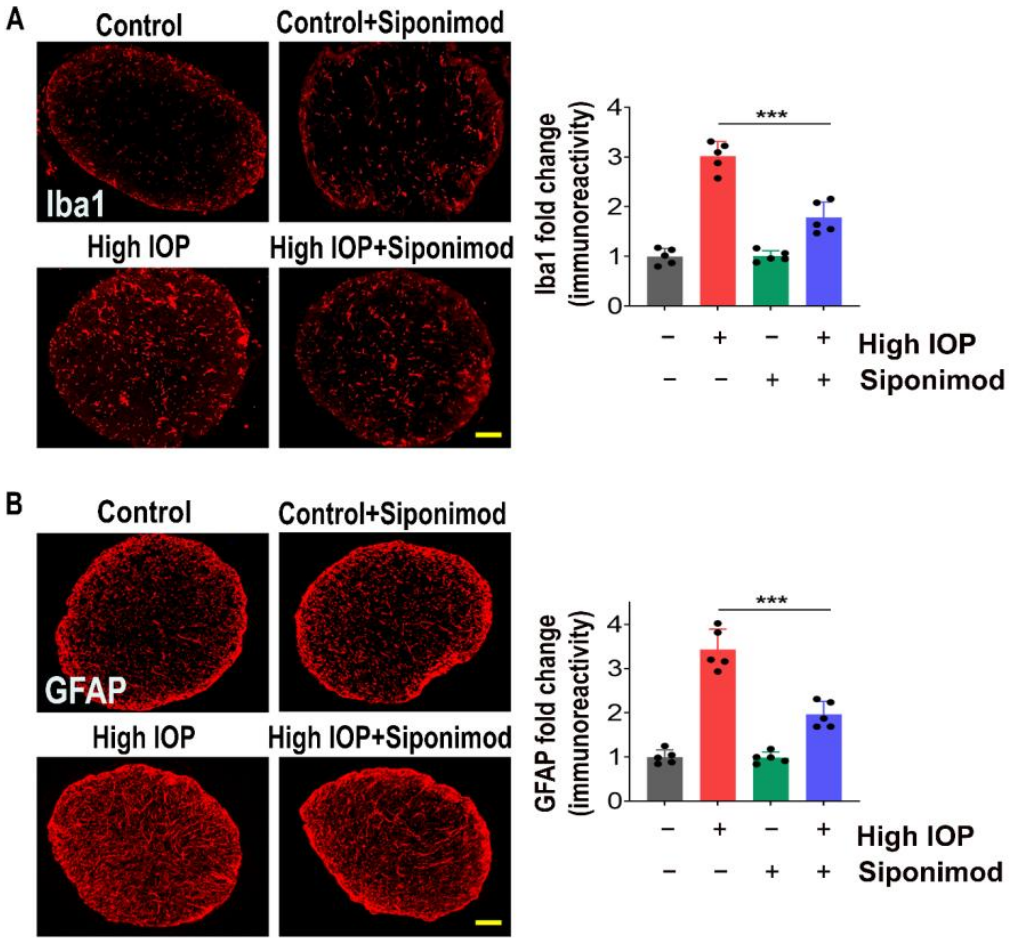

Additional Figure 1 Siponimod treatment reduced glial activation in optic nerves in chronic high IOP (8 weeks) condition.

(**A**) Representative immunofluorescence images of optic nerve cross-sections stained for microglia activation with Iba1 areas (red) and their quantification. (**B**) Analysis of GFAP stained (red) for reactive astrogliosis in ONs and their immunoreactivity measurements (scale bar: 50 μm). Data are expressed as the mean ± SD. ***$P < 0.001$ (one-way analysis of variance with Tukey's multiple comparisons test, $n = 5$ ONs per group). GFAP: Glial fibrillary acidic protein; Iba1: ionized calcium-binding adaptor molecule 1; IOP: intraocular pressure.

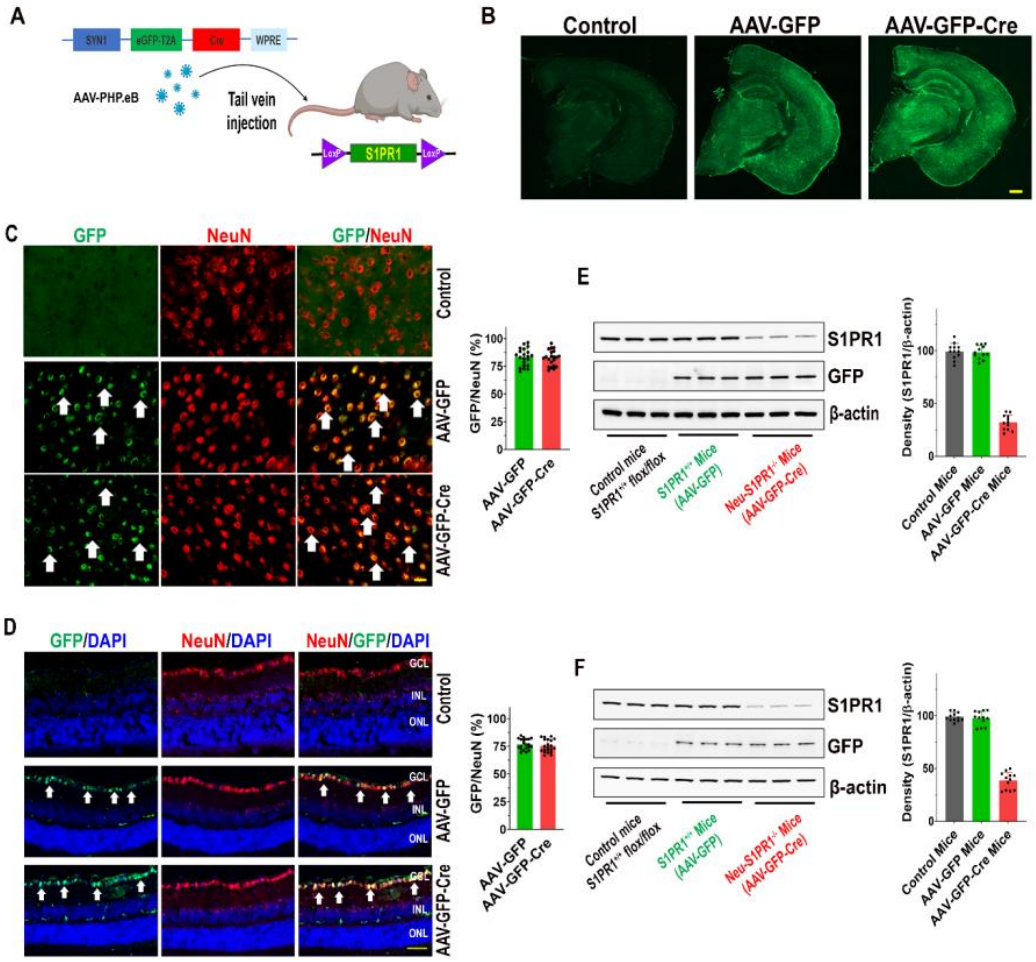

Additional Figure 2 Neuronal specific deletion of S1PR1 using *AAV-PHP.eB-Syn1-GFP-Cre* in S1PR1$^{flox/flox}$ transgenic mice.

(**A**) Schematic view depicting the GFP-Cre recombinase expression under neuron-specific promoter Syn1 integrated into the AAV-PHP.eB vector followed by tail vein injection of the viral particles into S1PR1$^{flox/flox}$ transgenic mouse strains. (**B**) Efficient transduction across the brain was evident by GFP marker (green) expression (scale bar: 500 µm). (**C**) Representative images of immunohistochemistry stained for GFP (green) and neuron-specific staining NeuN (red) (arrows indicate the GFP expression in neurons) and bar graph showing transduction efficiency quantified by the percentage of GFP$^+$ cells to the total NeuN cells (colocalization of GFP in neurons) in the dorsolateral geniculate nucleus (dLGN) of the brain (n = 20 per group, scale bar: 20 µm). (**D**) Representative retinal sections stained for GFP (green) and NeuN (red), DAPI (blue), and their quantification for transduction efficiency (arrows indicate the GFP expression in RGCs) (n = 20 per group, scale bar: 50 µm). (**E**) Western blot analysis of the brain dLGN tissue and densitometry quantification showing deletion of S1PR1 (n = 12 per group). (**F**) Western blot analysis of the retinal tissue and densitometric quantification for S1PR1 deletion (n = 12 per group). AAV: Adeno-associated virus; DAPI: 4',6-diamidino-2-phenylindole; S1PR: sphingosine-1-phosphate receptor.

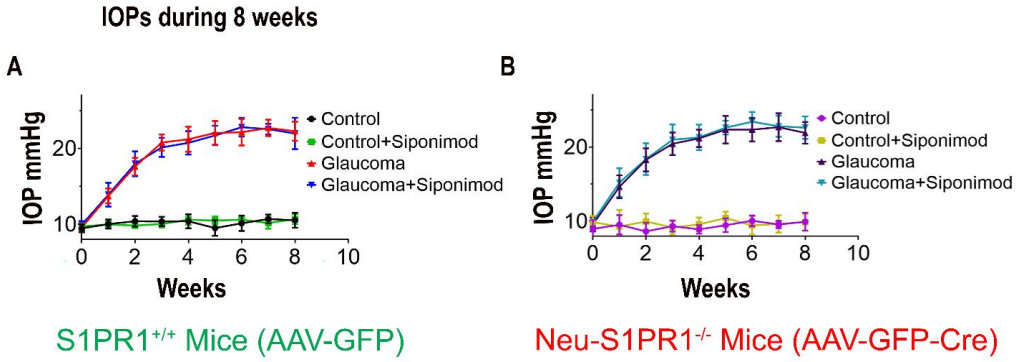

Additional Figure 3 Chronic IOP elevation in different group mice eyes for 8 weeks following microbead injections.

(**A**) Control S1PR1$^{+/+}$ mice injected with AAV-Syn1-GFP and (B) neuronal S1PR1$^{-/-}$ (Neu-S1PR1$^{-/-}$) mice injected with AAV-Syn1-GFP-Cre recombinase (n = 10 per each group). AAV: Adeno-associated virus; IOP: intraocular pressure; S1PR: sphingosine-1-phosphate receptor.

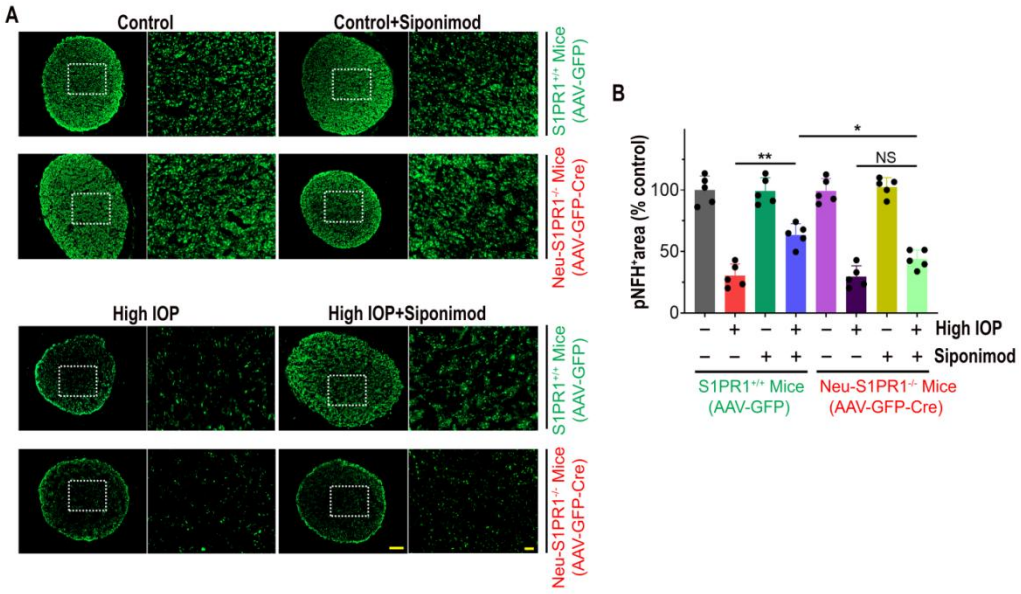

Additional Figure 4 Effects of siponimod on optic nerve damage under optic nerve injury induced by high IOP (8 weeks) in control and Neu-S1PR1$^{-/-}$ (AAV-GFP-Cre) mice groups.

(**A**) Immunofluorescence staining of cross-section of optic nerves for phosphorylated neurofilament heavy-chain (pNFH, green) (representative, scale bar: 50 μm) and measurements of immunoreactivity (scale bar: 10 μm) from magnified areas (boxes) of ONs. (**B**) Quantification of pNFH^{+} areas in different mice groups (NS, not significant, *P < 0.05, **P < 0.01, n = 5 per group). Statistical significance was determined using one-way analysis of variance with Tukey's multiple comparisons test (mean ± SD). AAV: Adeno-associated virus; IOP: intraocular pressure; S1PR: sphingosine-1-phosphate receptor.

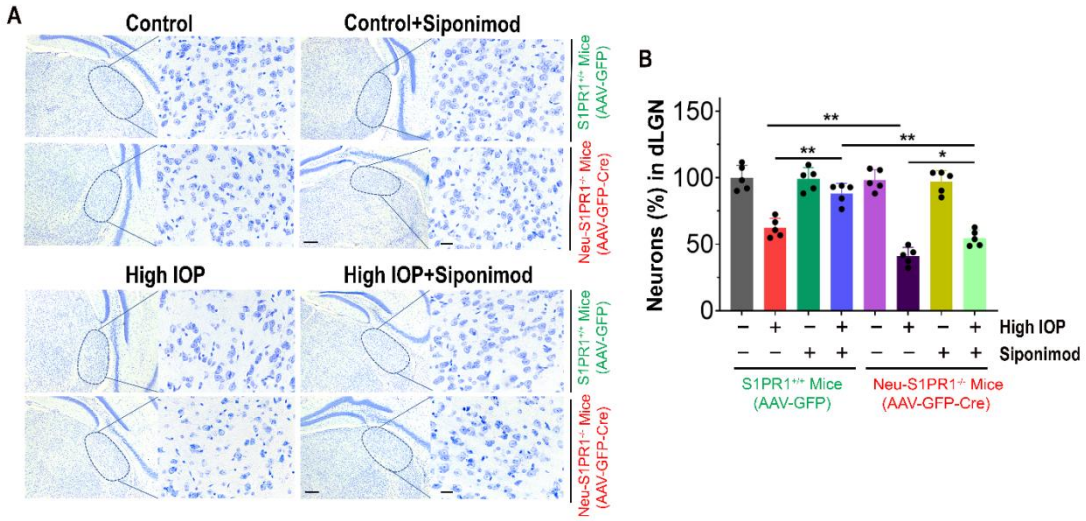

Additional Figure 5 Effects of neuronal-specific S1PR1 deletion on dorsolateral geniculate nucleus (dLGN) degenerative changes under chronic IOP condition (8 weeks).

(**A**) Nissl staining of coronal sections (contralateral) of mouse brains. Marked is the dLGN region of the brain used to quantify the neuronal density (representative, Scale bars: 200 μm) in control and Neu-S1PR1$^{-/-}$ (AAV-GFP-Cre) mice groups. Neuronal counts were measured from magnified images of the dLGN regions (scale bars: 20 μm). (**B**) Quantification of neuronal density among different mice groups (*P < 0.05, **P < 0.01, n = 5 per group). Statistical significance was determined using one-way analysis of variance with Tukey's multiple comparisons test (mean ± SD). AAV: Adeno-associated virus; IOP: intraocular pressure; S1PR: sphingosine-1-phosphate receptor.

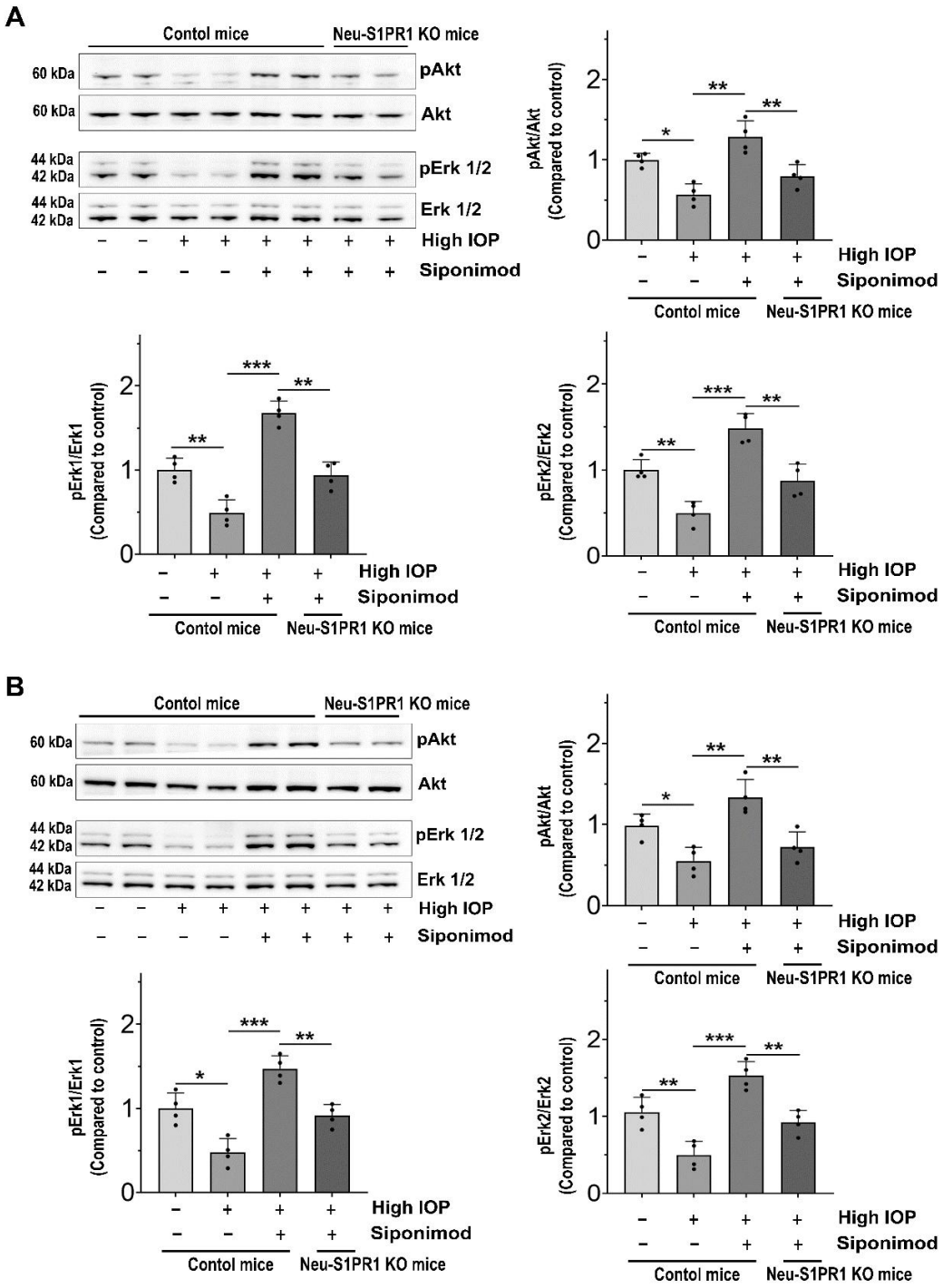

Additional Figure 6 Deletion of S1PR1 in neurons reduces siponimod mediated upregulation of pro-survival signaling pathways Akt and Erk1/2 in the retina and brain.

(A) Western blot analysis of Akt (phsopho-S473 antibody) and Erk1/2 (Phospho-p44/42 MAPK (Erk1/2) (Thr202/Tyr204) phosphorylation levels in retinas and (B) in the dorsolateral geniculate nucleus (dLGN) region of the brain tissues and their densitometric quantitative analysis in control S1PR1$^{+/+}$ and Neu-S1PR1$^{-/-}$ (AAV-GFP-Cre) mice under normal and high IOP (8 weeks) conditions (*P < 0.05, **P < 0.01, ***P < 0.001, n = 4 per group). Statistical significance was determined using one-way analysis of variance with Tukey's multiple comparisons test (mean ± SD). AAV: Adeno-associated virus; IOP: intraocular pressure; S1PR: sphingosine-1-phosphate receptor.

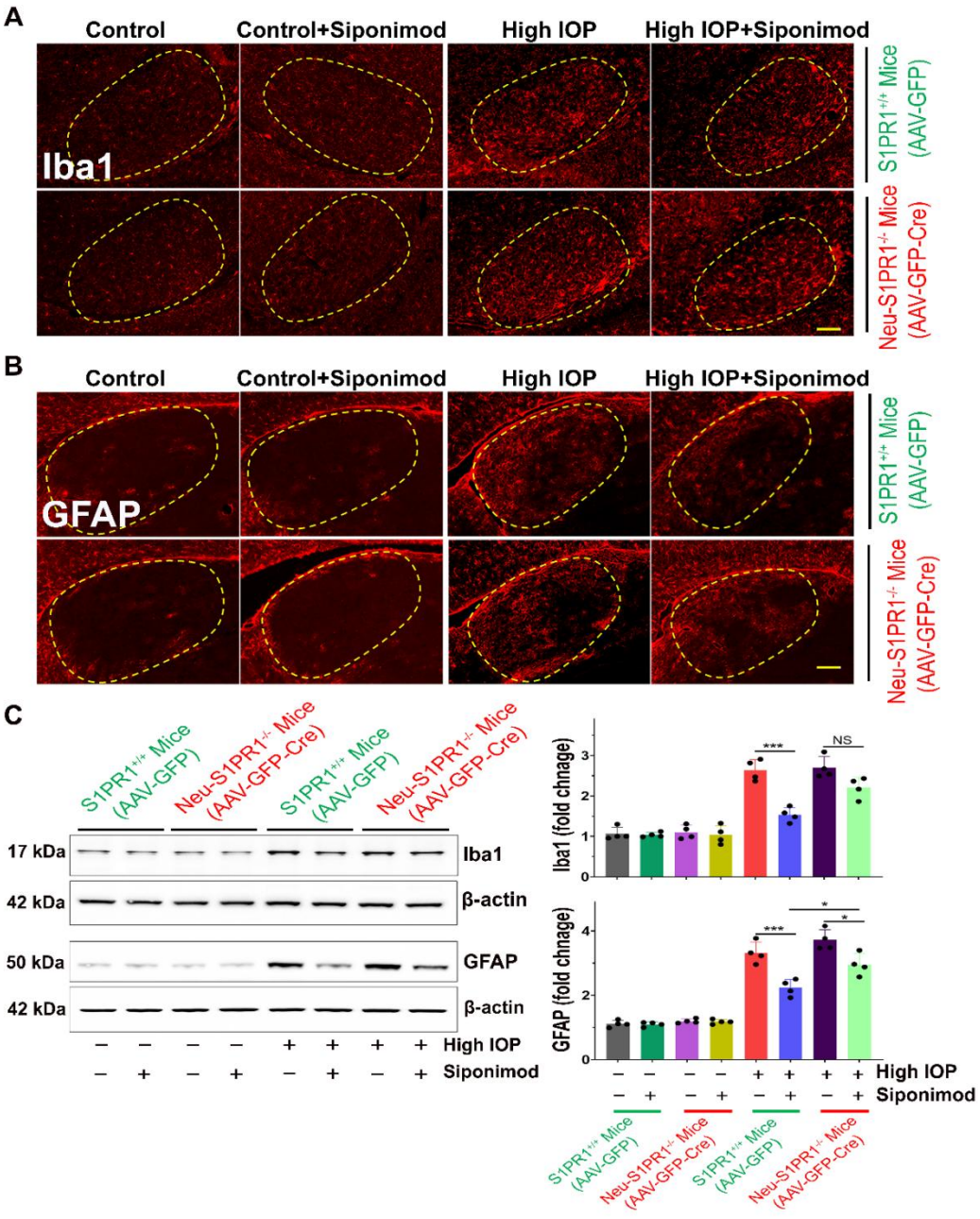

Additional Figure 7 Siponimod suppresses microglial activation and reactive astrocytes in dLGN in control mice and its protective effect is reduced in Neu-S1PR1$^{-/-}$ (AAV-GFP-Cre) mice in chronic optic nerve injury condition.

(A) Representative immunofluorescence images of coronal sections of different mouse groups' brains (contralateral, dLGN region is marked with a dotted circle, scale bar: 100 μm) stained for microglial activation with Iba1 antibody (red) and (B) reactive astrocytes with GFAP (red) in control and Neu-S1PR1$^{-/-}$ mice groups. (**C**) Western blot analysis and their quantification for Iba1 and GFAP expression in dLGN (NS: not significant, *P < 0.05, ***P < 0.001, n = 4 per group). Statistical significance was determined using one-way analysis of variance with Tukey's multiple comparisons test (mean ± SD). AAV: Adeno-associated virus; dLGN: dorsolateral geniculate nucleus; IOP: intraocular pressure; S1PR: sphingosine-1-phosphate receptor.

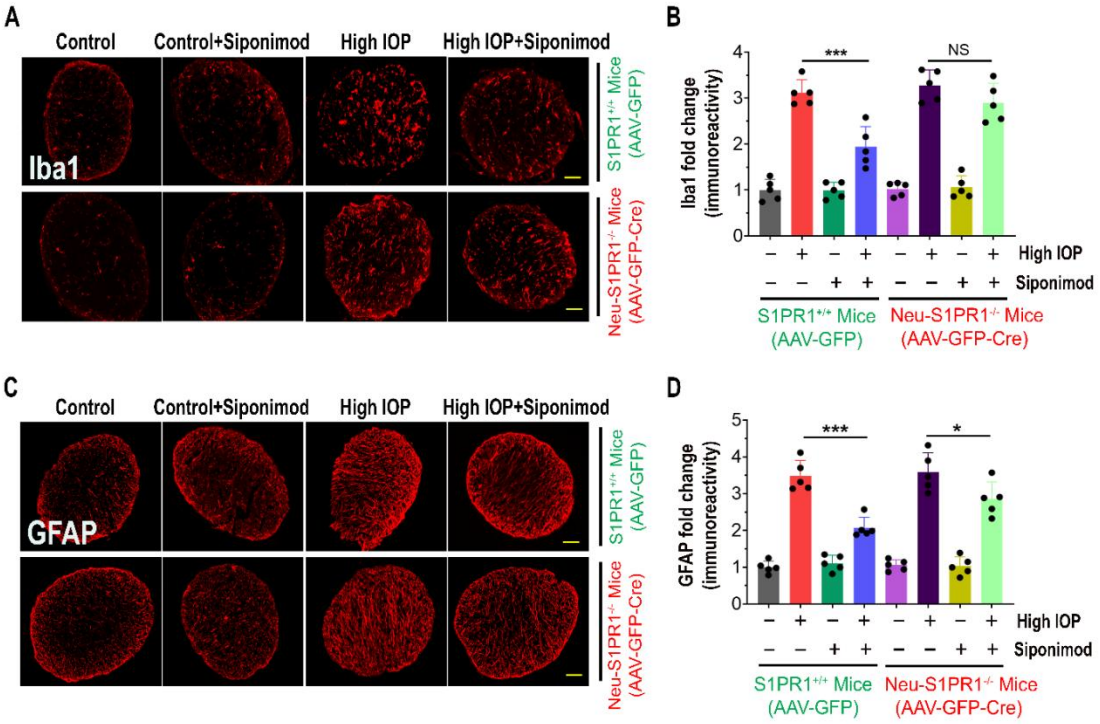

Additional Figure 8 Effects of siponimod on glial activation in optic nerve under high IOP (8 weeks) induced optic nerve injury.

(A) Representative immunofluorescence staining of optic nerve-cross sections stained with Iba1 (red) for microglial and (B) their quantitative analysis of Iba1^{+}areas. (C) ON sections stained with GFAP (red) for reactive astrogliosis and (D) their quantitative immunoreactivity analysis (scale bar: 50 μm) in control and Neu-S1PR1$^{-/-}$ (AAV-GFP-Cre) mice groups. NS: not significant, $*P < 0.05$, $***P < 0.001$, $n = 5$ ONs per group. Statistical significance was determined using one-way analysis of variance with Tukey's multiple comparisons test (mean ± SD). AAV: Adeno-associated virus; GFAP: glial fibrillary acidic protein; Iba1: ionized calcium-binding adaptor molecule 1; IOP: intraocular pressure; S1PR: sphingosine-1-phosphate receptor.

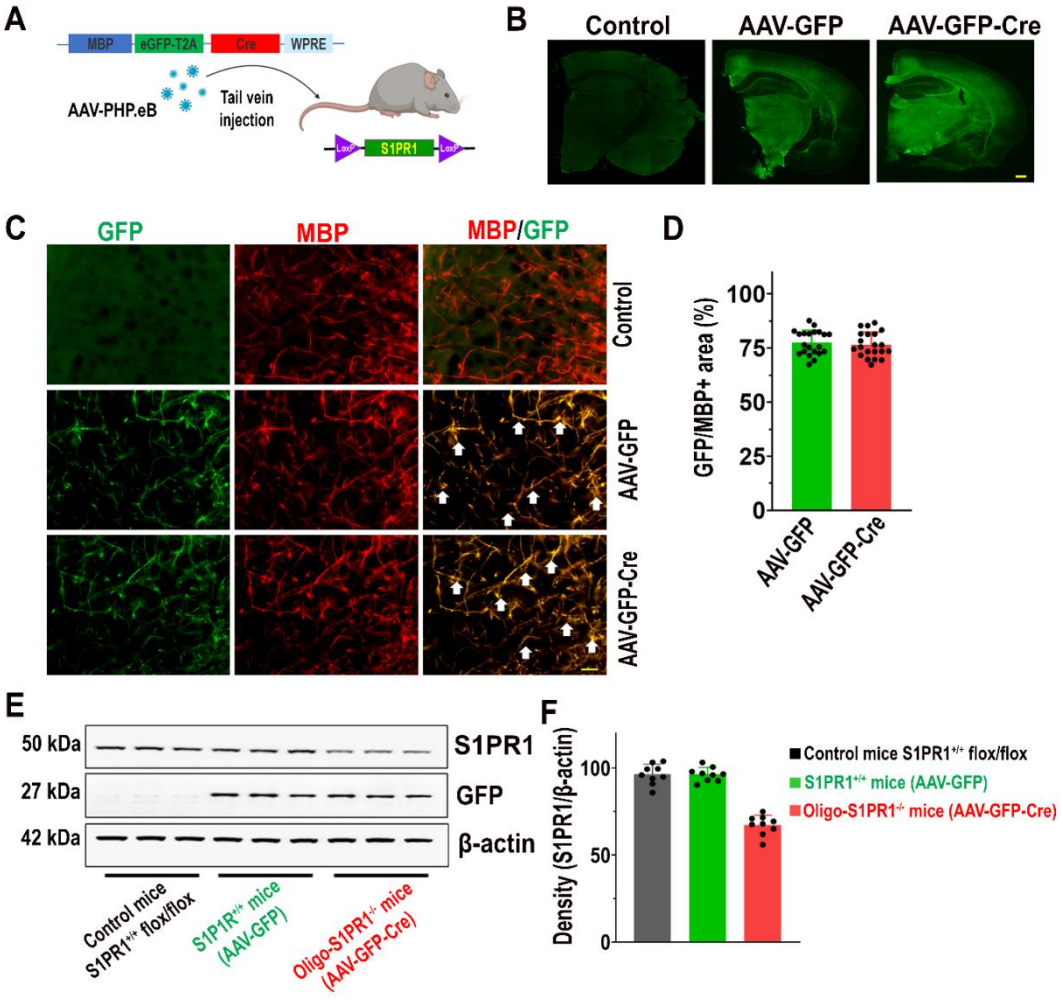

Additional Figure 9 Transduction and specific deletion of S1PR1 in oligodendrocytes using AAV-PHP.eB-MBP-GFP-Cre in S1PR1$^{flox/flox}$ transgenic mice.

(A) Schematic view depicting the GFP-Cre recombinase expression under Oligodendrocytes specific promoter MBP integrated into the AAV-PHP.eB vector followed by tail vein injection of the viral particles into S1PR1$^{flox/flox}$ transgenic mouse strains. (B) Transduction across the brain is evident by the GFP marker (green) expression (scale bar: 500 μm). (C) Representative images of immunohistochemistry stained for GFP (green) and Oligodendrocytes specific staining MBP (red) showing oligodendrocytes specific expression of GFP colocalization (arrows) with MBP in the brain (scale bar: 20 μm). (D) Transduction efficiency quantified by the percentage of GFP$^+$ area to the total MBP area in the dorsolateral geniculate nucleus (dLGN) of the brain (n=20 per group). (E) Western blot analysis of the brain dLGN tissue and (F) densitometry quantification showing deletion of S1PR1 (n = 9 per group). AAV: Adeno-associated virus; MBP: myelin basic protein; S1PR: sphingosine-1-phosphate receptor.

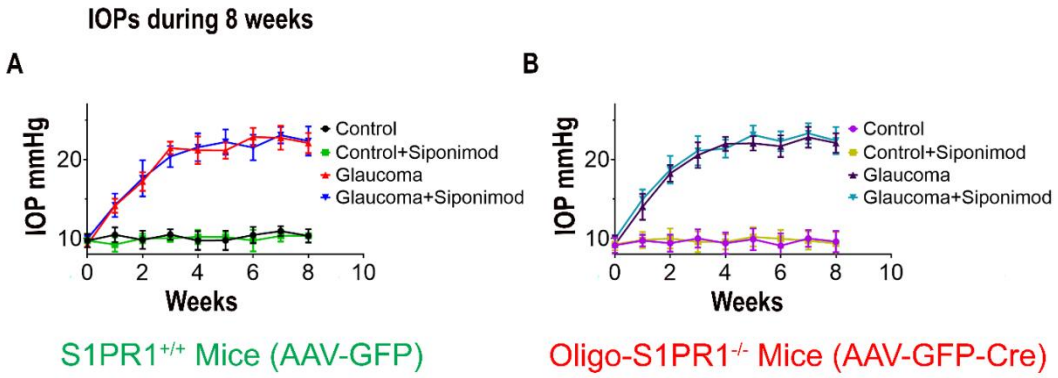

Additional Figure 10 Chronic IOP elevation in different group mice eyes for 8 weeks following microbead injections.

(**A**) Control (S1PR1$^{+/+}$) mice injected with AAV-MBP-GFP and (**B**) Oligodendrocytes S1PR1$^{-/-}$ mice injected with AAV-MBP-GFP-Cre recombinase (mean ± SD, n = 9 per each group). IOP: Intraocular pressure; S1PR: sphingosine-1-phosphate receptor.

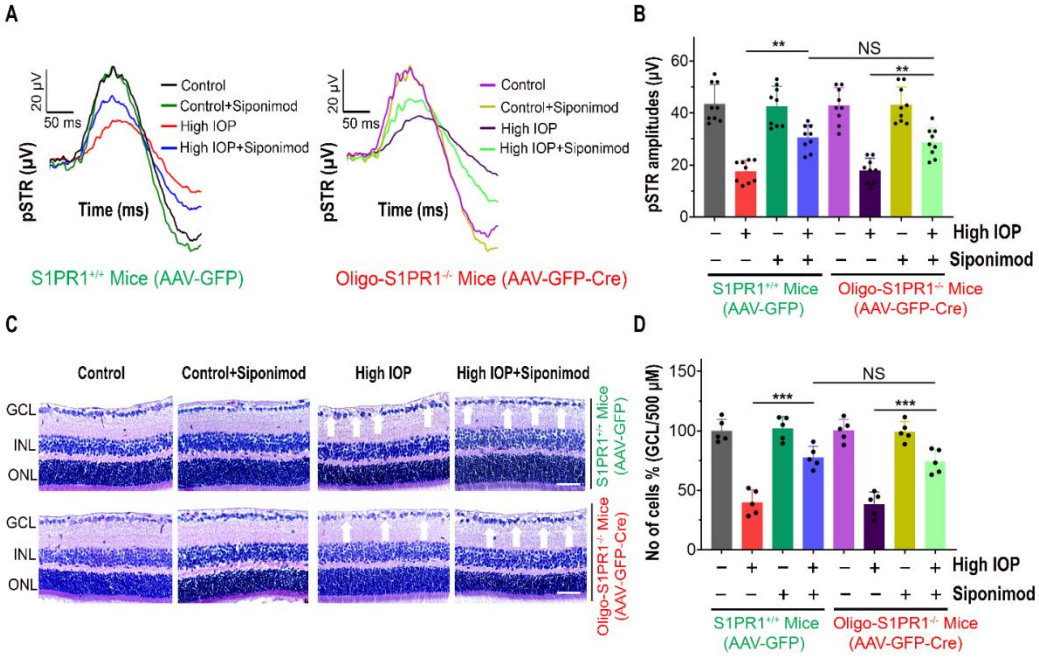

Additional Figure 11 Effects of oligodendrocyte-specific S1PR1 deletion on retinal degenerative changes under chronic IOP condition.

(A) Positive scotopic threshold responses (pSTR) and (B) quantification of the pSTR amplitudes of control and high IOP eyes of control (AAV-MBP-GFP) and Oligo-S1PR1$^{-/-}$ (AAV-MBP-GFP-Cre) mice treated with/without siponimod (**P < 0.01, n = 9 per group). (C) H and E staining of retinal cross-sections (representative, arrows indicate changes in the cell densities, scale bars: 50 μm; GCL: ganglion cell layer; INL: inner nuclear layer; ONL: outer nuclear layer) and (D) cell counts in the GCL of control and Oligo-S1PR1$^{-/-}$ mice under normal and high IOP conditions (NS: not significant, ***P < 0.001, n = 5 per group. Statistical significance was determined using one-way analysis of variance with Tukey's multiple comparisons test (mean ± SD). AAV: Adeno-associated virus; IOP: intraocular pressure; S1PR: sphingosine-1-phosphate receptor.

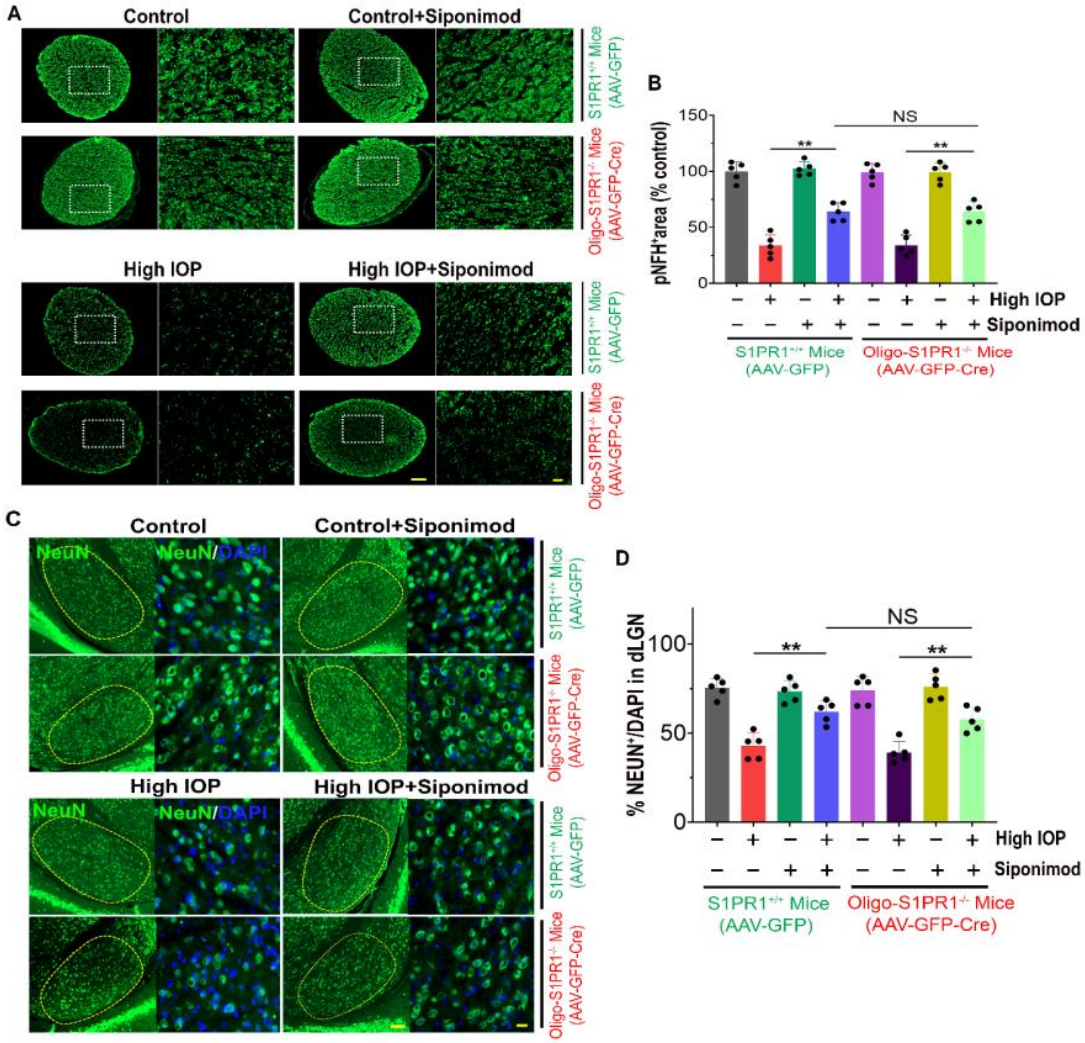

Additional Figure 12 Effects of oligodendrocyte-specific deletion of S1PR1 on the optic nerve and dLGN neurodegeneration under high IOP (8 weeks) optic nerve injury condition.

(A) Immunofluorescence staining of cross-section of optic nerves for phosphorylated neurofilament heavy-chain (green, pNFH) (scale bar: 50 μm) and measurements of immunoreactivity (scale bar: 10 μm) from magnified areas (boxes) of ONs of control and Oligo-S1PR1$^{-/-}$ mice groups. (B) Quantification of pNFH^{+} areas in different mice groups. (C) Representative immunofluorescence images of coronal sections of mouse brains (contralateral) stained with anti-NeuN (green), a neuronal marker, and DAPI (blue) (scale bar: 100 μm) and the dLGN region is marked with dotted circles in control and Oligo-S1PR1$^{-/-}$ mice groups. (D) Quantification of the percentage of NeuN^{+} cells out of DAPI-positive cells in the dLGN from magnified areas (scale bar: 20 μm) among mice groups. NS: Not significant. $^{**}P < 0.01$, n = 5 per group. Statistical significance was determined using one-way analysis of variance with Tukey's multiple comparisons test (mean ± SD). AAV: Adeno-associated virus; dLGN: dorsolateral geniculate nucleus; IOP: intraocular pressure; S1PR: sphingosine-1-phosphate receptor.